Department of Biomedical Sciences

University of Veterinary Medicine Vienna

Institute of Pharmacology and Toxicology

(Head: Univ.-Prof. Dr.med.univ. Veronika Sexl)

Sterol Endoperoxides: Synthesis, Reactions and Antileishmanial Activity

Bachelor thesis submitted for the fulfilment of the requirements for the degree of

Bachelor of Science (BSc.)

University of Veterinary Medicine Vienna

submitted by

Moris Ahmetasevic

Vienna, 16.11.2022.

Acknowledgements

Hereby, I would like to express my gratitude to Prof. Dr. Lars Gille for his continual support, using his expertise and patience to supervise me throughout the whole process. I would also like to thank everyone at the Institute of Pharmacology and Toxicology at the University of Veterinary Medicine in Vienna, especially Prof. Dr. Katrin Staniek, for providing an enjoyable working atmosphere.

This would have not been possible without the support of my family and my girlfriend, who have been instrumental during this journey, and without whom I would have not managed to reach this stage in my life.

We acknowledge the support of this work by Dr. Markus Bacher from the Institute of Chemistry of Renewable Resources (University of Natural Resources and Life Sciences, Vienna) for NMR analysis of sterol derivatives. Furthermore, we acknowledge the financial support for this work by the Austrian Science Fund (FWF) under grant P 27814-B22.

Table of Contents

1. Introduction 5
1.1 *Leishmania spp.* 5
1.1.2 Leishmaniasis 6
1.1.3 Therapeutical approaches 6
1.2 Endoperoxides as antileishmanial agents 7
1.3 Sterols 7
1.3.1 Ergosterol (Ergo) 8
1.3.2 7-Dehydrocholesterol (DHChol) 8
1.4 Cycloaddition of oxygen 9
1.4.1 Ergosterol peroxide (ErgoEP) 9
1.4.2 7-Dehydrocholesterol peroxide (DHCholEP) 9
1.5 The problems of research on ErgoEP and DHCholEP 10
1.6 Aims of study 10
2. Materials and Methods 12
2.1 Chemicals 12
2.1.2 Structures of endoperoxides and their analogs 13
2.2 LtP Cell Culture 14
2.3 LtP Viability assay 14
2.4 Synthesis of ErgoEP and DHCholEP 15
2.5 Chromatography 16
2.5.1 Thin-layer chromatography (TLC) 16
2.5.2 Vacuum Liquid Chromatography (VLC) 16
2.6 Formation of the xylenol/Fe^{3+} complex by EP 18
2.7 Simulation of NMR spectra 19
2.8 Experimental NMR 19
3. Results 20
3.1 Basic ^{1}H NMR spectra prediction 20
3.2 Synthesis 25
3.3 Reaction monitoring 27
3.4 ^{1}H NMR of educts and products 32
3.5 Viability 36
3.6 Reaction of EP with Fe^{2+} 40

4. Discussion 42
5. Summary 48
6. Abbreviations 49
7. References 51
8. List of figures 54
9. List of tables 56

1. Introduction

1.1 *Leishmania spp.*

Leishmania are single-celled protozoan parasites that cause a disease known as Leishmaniasis. Two different life forms of *Leishmania spp.* can be distinguished: a flagellated, motile form known as promastigotes and the non-motile amastigotes (1). Amastigotes reside as intracellular parasites of mammalian cells, mostly macrophages. The life-cycle of *Leishmania spp.* begins when a sandfly takes up the amastigotes from the blood of an infected mammal (2). The amastigotes transform to procyclic promastigotes and multiply in the midgut of a sandfly. They migrate towards the anterior midgut, where they transform into infective metacyclic promastigotes. During the next blood meal, the metacyclic promastigotes are inserted into a mammalian host, taken up by macrophages, and subsequently transformed into amastigotes inside the phagolysosome of the macrophages (Figure 1) (2).

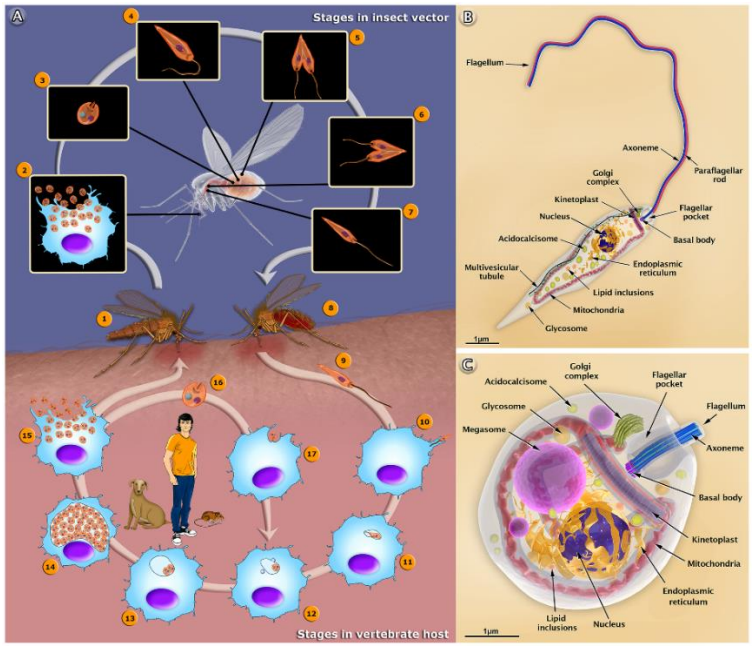

Figure 1. A: Life cycle of *Leishmania*. 1) Sandfly takes up amastigotes from an infected mammal. 2) Macrophages infected with amastigotes. 3) Amastigote. 4) Amastigotes transform into procyclic promastigotes. 5) Multiplication of the procyclic promastigotes in the midgut. 6) Migration of the procyclic promastigotes towards the anterior midgut where the cell division is re-initiated. 7) Promastigotes transform into

metacyclic promastigotes. 8) Sandfly releases metacyclic promastigotes. 9), 10), 11) Metacyclic promastigotes infect macrophages, where they transform into amastigotes. 12), 13), 14) Amastigotes multiply in the phagolysosome. 15) Amastigotes break out of the cell. 16), 17) After breaking out of the cell, amastigotes can re-infect the macrophages. B: morphological structure of promastigotes. C: morphological structure of amastigotes (2)

1.1.2 Leishmaniasis

Leishmaniasis is a disease caused via transmission of the infective form of *Leishmania spp.* from a sandfly to a mammalian host. Therefore, it is endemic in places that are considered to be the natural habitat of a sandfly. That includes approximately 98 countries leaving more than 350 million people potentially exposed to the disease (3). Three different clinical forms can be differentiated: cutaneous (CL), mucocutaneous (MCL) and visceral leishmaniasis (VL) (4). CL, usually caused *by Leishmania mexicana, Leishmania braziliensis and Leishmania panamensis* shows low mortality and self-cures in 3–18 months, whereas VL caused by *Leishmania donovani* often leads to fatal consequences if not treated early. Besides humans, dogs were considered as an important reservoir of the disease in the Mediterranean and American region. Treating the leishmaniasis of dogs, specifically *Leishmania infantum* infection, plays an important role in reducing the incidence of human leishmaniasis (4). Speaking about all three clinical forms, WHO reports between 20000-30000 death cases with 0,9-1,6 million cases per year (5).

1.1.3 Therapeutical approaches

The first-line drugs in therapy of CL and VL are pentavalent antimonials: sodium stibogluconate (SSG), or meglumine antimoniate. The main disadvantages of the named therapeutics are high price, resistance development and diverse side effects which can be reduced by combining them with an alternative therapy (5). For the treatment of VL, the WHO Expert Committee has recommended the combination of SSG with paromomycin for 17 days in East Africa (6). Besides these, ambisome and miltefosine have also been used frequently. As for the CL type, the use of pentavalent antimonials remains the most frequent therapy, as well as miltefosine. Amphotericin B was used in the treatment of more serious cases of CL, in which the above-mentioned medicaments have not yielded expected results (6).

1.2 Endoperoxides as antileishmanial agents

Endoperoxides (EP) are a class of drugs that can be potentially used in the treatment of various parasitic diseases, such as malaria and leishmaniasis (7). In fact, artemisinin (Art) and its derivatives are the most effective antimalarials. However, there have been some signs of resistance development against these drugs in western Cambodia, which furthermore inspires new drug development and possible combination therapy development (9). They are characterized by a peroxidic bridge in form of an O-O single bond (23). What differentiates this group from hydroperoxides, is the ability to partially evade the detoxification system of the mammalian host cell, therefore, exerting their antileishmanial function inside the phagolysosome of infected macrophages. EP relevant for the treatment of Leishmaniasis are Art, ascaridole (Asc) (7) and anthracene EP (AcEP) (8). It is believed that the activation of these EP occurs through single electron reduction leading to radical formation. Asc exhibited much lower IC_{50} values over its non-peroxidic analog 1,4-cineole (Cin) in *Leishmania tarentolae* promastigotes (LtP). Likewise, Art has shown even higher toxicity in LtP as opposed to macrophages (7). It has also been shown, that Asc is being transformed into radicals by Fe^{2+} and hemin in the presence of reductants, suggesting that Fe^{2+} has a significant role in the activation of Asc. Iron presents a very important survival factor for protozoal parasites. The amastigotes that reside in macrophages, which are involved in the process of erythrophagocytosis, usually get enough iron supply from heme degradation. In addition, the parasites have found various ways to obtain sufficient levels of iron from other sources (9). AcEP were produced via the reaction of substituted anthracenes with singlet oxygen by photo-oxidation, and were used for technical purposes, such as oxygen carriers or photolithography. A recent study suggests that certain AcEP can have cytotoxic functions in LtP via the formation of carbon-centered radicals under the influence of Fe^{2+}, similar to Art and Asc (8).

1.3 Sterols

Sterols are a group of tetracyclic triterpenoid lipids that have major functions in eukaryotic organisms such as influencing membrane fluidity, stress tolerance hormons and cell signaling (10). They can be classified into two major groups: phytosterols and zoosterols. A widely known representative of sterols is cholesterol (Chol), which belongs to the group of

zoosterols. Ergosterol (Ergo), with a structure related to Chol, can be found in fungi and protozoa (11). Phytosterols were clinically tested as potential nutritional supplements, that could inhibit the absorption of Chol and therefore provide health benefits (12). Chol consists of four rings, with a single hydroxyl group attached to C3, an alkyl group attached to C17 and a singular double bond at 5,6-position (14). It can take up to 50 % of the membrane lipid composition depending on the membrane and plays an important role in maintaining the membrane fluidity (13). Besides above-mentioned functions, Chol can also be a target of oxidation reactions by ROS in cells, resulting in the formation of peroxyl radicals and oxidatively modified cholesterol derivatives. The initiation of this reaction is the process of the C7 hydrogen abstraction by lipid peroxyl radicals ($LOO^{\cdot}$). The carbon-hydrogen bond at the mentioned position is weaker, which leads to enhanced reactivity (13). Subsequently, we focus on sterols used in this work.

1.3.1 Ergosterol (Ergo)

Structurally, Ergo differs from Chol by having an additional double bond at the 7,8-position, a double bond in the alkyl chain at 22,23-position and a methyl group bound to C24 (15) (See Figure 2). *Leishmania spp.* lack enzymes that produce Chol and, therefore, produce Ergo, the function however remains very similar. In addition, Leishmania parasites acquire substantial amounts of cholesterol from their environment (19). One function of Ergo is maintaining the fluidity of the membrane. Medicaments, such as Amphotericin B can specifically bind to Ergo in parasite membranes and disrupt the fluidity and osmotic properties of the membrane (16). Ergo has also been proven as an essential growth factor of the fungi (17).

1.3.2 7-Dehydrocholesterol (DHChol)

DHChol is a sterol similar to Chol. The only structural difference to Chol is the lack of hydrogen at C7, resulting in a formation of an additional double bond at the 7,8-position. The biological relevance of DHChol lies in the fact that it is a precursor of Vitamin D. The transformation of DHChol to Vitamin D3 is not influenced by the enzymes (18). There is a reported functional use as an emulsion stabilizing, skin conditioning and viscosity increasing agent (19). Due to an additional double bond, the susceptibility to oxidation in comparison to Chol increases drastically (20).

1.4 Cycloaddition of oxygen

The reaction of two unsaturated molecules under the formation of a cyclic adduct is referred to as cycloaddition. The reactions considered in this work are [4+2] cycloadditions including a diene (4 electrons, in Ergo and DHChol) and singlet oxygen (2 electrons in $^1O_2$) forming a six-membered ring including oxygen (the peroxide group). Singlet oxygen in these reactions is often generated by irradiation of photosensitizers (PS). Through photo-oxidation reactions catalyzed by PS, such as eosin, it is possible to transform Ergo into ergosterol peroxide (ErgoEP). A PS dye, in presence of molecular oxygen, can initiate the photochemical reactions while absorbing the UV-Vis light. These reactions lead to the formation of singlet oxygen, which can furthermore catalyze the transformation of Ergo into ErgoEP (21). A PS is essential in this reaction, as it absorbs energy which is subsequently transferred to molecular oxygen, leading to the formation of singlet oxygen. Besides eosin, methylene blue (MB) and Bengal rose are also frequently used in these reactions. One of the PS found in nature is macrosporin (22). Produced by the plant-pathogenic fungus *Stemphylium lycopersici*, it causes cell necrosis via the formation of singlet oxygen, that furthermore leads to the destabilization of the cell membrane and enzyme deregulation (22).

1.4.1 Ergosterol peroxide (ErgoEP)

Originally isolated from *Aspergillus fumigatus*, ErgoEP possesses anti-angiogenic and cytotoxic properties (24), acting as an inhibitor of tumor growth (23). The peroxide group between C5 and C8 differentiates it from Ergo. Besides the anti-tumor function, this molecule has an antibacterial function as well, showing high killing potential for *M. tuberculosis* (25). Although many studies report the cytotoxic function of ErgoEP against different cancer types, including breast cancer cellular models, the mechanism of function has never been fully discovered. There has been an effort to uncover the exact mechanism by creating ErgoEP chemical probes and using diverse live cell imaging studies. Although the results of the study have given some answers, further validation studies are needed (26).

1.4.2 7-Dehydrocholesterol peroxide (DHCholEP)

In comparison with its analogous counterpart ErgoEP, there are very few studies that examine the cytotoxic properties of DHCholEP. In fact, DHCholEP shows higher anti-cancer potency and selectivity than ErgoEP (27). The study has pointed out that DHChol lacks

cytotoxic functions, implying that the cytotoxic behavior of DHCholEP is being initiated by the peroxide group.

1.5 The problems of research on ErgoEP and DHCholEP

For most biochemical studies ErgoEP was isolated from natural sources, such as certain mushrooms. Although the reported purity of the resulting products was verified by NMR, the amount of ErgoEP often required large amounts of these natural sources and a long tedious workup procedure. Commercial availability of ErgoEP is hampered by its price (> 100 Euro/mg) which limits affordable amounts for experiments on the 100 mg scale. For DHCholEP even no commercial source is available. Therefore, in this work, the photochemical synthesis of both peroxides was attempted. For both of these chemicals, the variable yield of EP synthesized using photo-oxidation methods is a problem. The production of ErgoEP from Ergo, using eosin in pyridine as a PS, yielded 64 % of the peroxide (28). DHCholEP was produced out of DHChol using several different PS in different solvents, and the highest yield was 81 % with the lowest yield of 40 % (27). In order to perform various *in vitro* experiments, adjusting the conditions of the production process is necessary, so that higher yields and sufficient purity are achieved. As a consequence of a low number of studies regarding the synthesis of ErgoEP and DHCholEP, there are no clear indications as to which setup in the production process offers the best results. In addition, the photo-oxidation techniques can produce different side products, which can negatively affect the purity of the end product.

1.6 Aims of study

- Evaluation of ^{1}H NMR spectra of sterols to monitor the purity of synthetic products
- Establishment of synthesis and purification procedures for ErgoEP and DHCholEP
- Study of antileishmanial properties of both EP and determination of IC_{50} values for their influence on viability in the cell model of LtP.
- Examining in part the antileishmanial mechanism of both EP by performing viability assay for LtP in the absence and presence of N-acetyl cysteine (NAC) as a radical scavenger. If the mechanism of action of sterol EP against Leishmania

is mediated by the formation of carbon-centered radicals, NAC should interfere in the anti-leishmanial effect of sterol EP by increasing the IC_{50} values.

- Study the reaction rate of ErgoEP and DHCholEP with Fe^{2+} in comparison to Ergo and DHChol as well as other reference compounds using spectrophotometric methods and the xylenol orange (XO) assay to explore possible EP activation pathways.

2. Materials and Methods

2.1 Chemicals

All of the chemicals used in the preparation, maintenance and synthetic processes are listed below:

Table 1. List of the chemicals used for preparation, maintenance and synthetic processes

Chemical	Supplier
Ascaridole (Asc)	Self-synthetized (34)
7-Dehydrocholesterol (DHChol)	Sigma-Aldrich (St. Louis, Missouri, USA)
Brain Heart Infusion medium (BHI)	Sigma-Aldrich (St. Louis, Missouri, USA)
Butylated hydroxytoluene (BHT)	Roche (Basel, Switzerland)
$CaCl_2$	Merck (Darmstadt, Germany)
CH_2Cl_2	Carl Roth (Karlsruhe, Germany)
$CHCl_3$	Merck (Darmstadt, Germany)
Cholesterol (Chol)	Sigma-Aldrich (St. Louis, Missouri, USA)
Dimethyl sulfoxide (DMSO)	VWR (Radnor, Pennsylvania, USA)
Eosin Y (EY)	Sigma-Aldrich (St. Louis, Missouri, USA)
Ergosterol (Ergo)	Acros Organics (Geel, Belgium)
Ethanol (EtOH)	Scharlab (Barcelona, Spain)
Ethyl acetate (EtOAc)	Carl Roth (Karlsruhe, Germany)
Glucose monohydrate (Glu)	Merck (Darmstadt, Germany)
H_2SO_4	Merck (Darmstadt, Germany)
Hemin	Sigma-Aldrich (St. Louis, Missouri, USA)
K_2HPO_4	Merck (Darmstadt, Germany)
KH_2PO_4	Merck (Darmstadt, Germany)
Methanol (MeOH)	Merck (Darmstadt, Germany)
Methylene blue (MB)	Merck (Darmstadt, Germany)
N-acetylcysteine (NAC)	Thermo Fisher Scientific (Waltham, MA, USA)
NH_4FeSO_4	VWR (Radnor, Pennsylvania, USA)
NH_4SCN	VWR (Radnor, Pennsylvania, USA)
Penicillin-streptomycin solution	VWR (Radnor, Pennsylvania, USA)
Pentamidine (Pen)	Sigma-Aldrich (St. Louis, Missouri, USA)

Petroleum ether (PE)	Carl Roth (Karlsruhe, Germany)
Na_2HPO_4	Merck (Darmstadt, Germany)
Resazurin	Sigma-Aldrich (St. Louis, Missouri, USA)
Xylenol orange (XO)	Merck (Darmstadt, Germany)
Yeast extract (YE)	Amresco (Solon, Ohio, USA)

2.1.2 Structures of endoperoxides and their analogs

Figure 2 shows the structures of EP with their analogs, as well as the structure of the control substances used in the experiments.

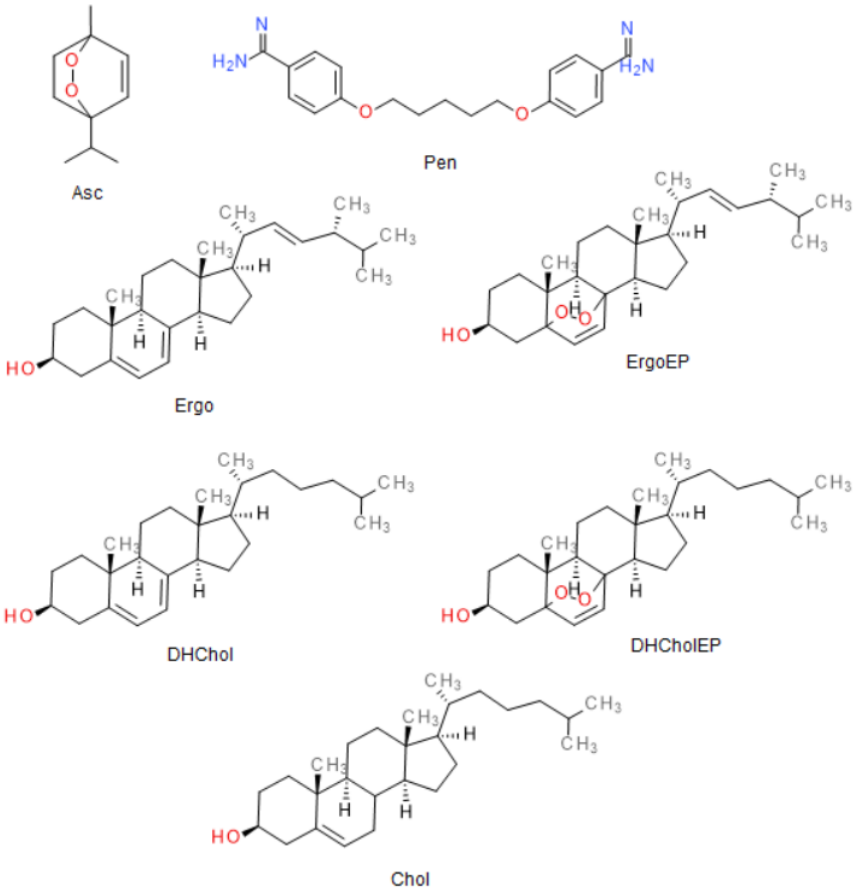

Figure 2. Structures and abbreviations of sterol EP, their analogs, as well as the control substances used in the experiments. Starting from above: ascaridole (Asc), pentamidine (Pen), ergosterol (Ergo), ergosterol peroxide (ErgoEP), 7-dehydrocholesterol (DHChol), 7-dehydrocholesterol peroxide (DHCholEP), cholesterol (Chol).

2.2 LtP Cell Culture

Leishmania tarentolae promastigotes (LtP) (strain P10 from Jena Bioscience, Germany) were employed as a biological system in tests performed in this work. The cells were cultivated in brain heart infusion (BHI) medium in 50 mL TubeSpin bioreactors. 5 mg/L of hemin was added to the tube, together with 50,000 IU/L of penicillin and 50 mg/L streptomycin to prevent contamination with bacteria. LtP were grown at 26.6 °C in an incubator (Cytoperm, Heraeus Instruments, Hanau, Germany), and cells were passaged three times a week. The cell number was calculated by measuring the optical density (OD) of the culture at 600 nm with a photometer (U-1100, Hitachi Ltd, Tokyo, Japan) and applying the formula $x*10^6$ cells/mL = OD_{600} * 0.969 * 124 (29). The target OD of the cells was set to 0.3, at Friday to 0.15 because of the longer incubation time during the weekend. So the expected cell density after the passage was $36*10^6$ LtP/mL, and $18*10^6$ LtP/mL on Fridays.

2.3 LtP Viability assay

In order to perform the viability assay, yeast extract medium (YEM) (20.7 g/L yeast extract powder, 1.2 g/L K_2HPO_4, 0.2 g/L KH_2PO_4, 2.9 g/L glucose monohydrate, pH 7.4) and PBS mixture was prepared (1:1, v/v). It also contained 25,000 U/L penicillin, 25 mg/L streptomycin, and 6 µM hemin (8). Additionally, a cell suspension containing $2*10^6$ LtP/mL in above mentioned YEM/PBS mixture was prepared. During this work, viability assays with two different dilution patterns in 96-well plates (flat bottom, sterile, non-treated, article number: 0030730011) (Eppendorf, Germany) were performed. In the first instance for vertical concentration gradients, 200 µL of YEM/PBS medium without LtP cells was distributed in the first row of a 96-well plate. Above mentioned cell suspension with LtP was distributed in the remaining wells. Afterwards, additional cell suspension and the examined volume of compound stocks were added to the last row of a plate. The concentration of the compounds in this row was adjusted to 200 µM, except for Pen (20 µM). This was followed by a 1:3 serial dilution up until the third row. The second row contained the cell suspension without compounds. For each compound, triplicates were measured, meaning that 4 compounds were analysed on a single 96-well plate. Combination assays with NAC were following the same protocol, however, the cell suspension on one half of the plate contained in addition 2 mM NAC, meaning that two test compounds were analyzed with and without the presence of NAC. In a second instance, the dilution was performed horizontally in 96-well plates and the

compounds were added to the first column of a plate. In this case, duplicates of each compound were measured, however, due to plate rearrangement more data points for the measurement of IC_{50} values of compounds were obtained. At first, 200 µL of YEM/PBS medium was placed in half of the wells of the first and second row, while the other wells were filled with 100 µL of the same medium. Additional medium, with the aliquots of compounds, was added to the first column, excluding the first and last row. Following this, 1:2 serial dilution was performed horizontally, after which the test wells were filled up with 100 µL of the LtP cell suspension. In both of these instances, 8 mL of PBS was placed between the wells to prevent the plate from drying out. After 48h hours of incubation time at 26.6 °C, 50 µL of resazurin was placed in each well (final concentration in each well 20 µM). Following 4 hours of incubation at 26.6 °C, the fluorescence was measured at 560 nm excitation and 590 nm emission using a plate reader (Perkin Elmer Enspire, Germany) (29).
A four-parameter logistic model was used to calculate the IC_{50} values using a custom-designed Excel worksheet with Python support (33). The mean of the fluorescence of all cell wells without compounds minus the respective mean of wells without cells (blank) was considered as 100% viability. The viability for wells with compounds was obtained by substracting their intensity by the blank intensity, dividing by the intensity for 100% viability and multiplying by 100. Afterwards, the viability/concentration relation was presented in form of a viability/concentration curve. The mean of each triplicate (for vertical concentration gradients) or duplicate (horizontal concentration gradients) measurement was considered as one data point, corresponding to the level of dilution (concentration).

2.4 Synthesis of ErgoEP and DHCholEP

For the synthesis of sterol EP, CH_2Cl_2 or EtOH was dried over $CaCl_2$ overnight, and a 50 mL aliquot was placed in a 100 mL two-neck round-bottom flask (32). Subsequently, 200 mg of sterol was stirred into the solvent using a magnetic stirrer. During the process, the solution was cooled down with ice. A constant flow of oxygen from an oxygen tank was introduced through a 0.9 x 120 mm cannula (Ehrhardt, Germany) into the reaction liquid. After 1 h, 5 mg of MB or 3 mg of EY was added to the mixture. Afterwards, the solution was irradiated for 20–60 minutes with two tungsten filament lamps placed 25 cm above the flask under a constant supply of oxygen. During this process, 200 µL aliquots were taken at different timestamps for evaluation by thin-layer chromatography (TLC). The liquid reaction mixture

was pooled with other reaction batches (in total three) of the same sterol/PS combination and stored at 4 °C until further purification of the products.

2.5 Chromatography

2.5.1 Thin-layer chromatography (TLC)

In order to evaluate the conversion process of sterols to their corresponding EP, TLC was used. During each synthesis process, samples at different time points were taken to monitor the progress of the reaction. Using glass capillary tubes, 5 µL samples of the aliquots were applied onto a 10x10 cm sheet of a TLC plate (TLC aluminum sheets with silica gel 60 F254, Art: No. 1.05554.0001) (Merck, Germany) and allowed to dry for at least 15 min. For equilibration 30 mL of mobile phase ($CHCl_3$ (97 % v/v) / MeOH (3% v/v)) was placed in a twin-trough TLC-developing chamber with a stainless-steel lid (VWR, USA). Then the plate was carefully placed inside the chamber and was developed until the eluent front line reached about 1.5 cm below the top of the plate. After the plate was taken out of the chamber, it was left for 20 minutes to dry, and afterwards it was illuminated with a high-pressure mercury UV-lamp with a 340 nm short-pass filter to visualize the spots.

2.5.2 Vacuum Liquid Chromatography (VLC)

After monitoring of the reaction progress for individual batches, these were pooled (three in total) and further purified using VLC. Initially, the solvent of the pooled fractions was subsequently evaporated using Rotavapor™ (Büchi, Switzerland) until approximately 50 mL of the solvent was left in the flask. About 2 g of Celite® 545 (VWR, USA) was added to the mixture, and the evaporation process was continued until the solvent was removed. For VLC, a glass column (20 x 400 mm, 125 mL capacity) with a sintered frit at the bottom and a vacuum connector (Lenz, Germany) was used. The column was loaded starting with filter paper discs and then silica gel (0.02 – 0.045 mm) (Carl Roth, Germany) up to a height of about 18 cm. Then the silica gel was compressed and over-layered by another filter paper disc, the Celite with our crude products and finally sea sand. The filled column was placed on top of a dripping funnel and a vacuum pump was connected to the column. Then the stationary phase was saturated with 60 mL of PE. Gradient elution of the column was performed using different volumes of PE and EtOAc (Table 2). The fractions were collected

in 20 mL glass tubes. From each fraction, 1 mL was transferred to 1.5 mL Eppendorf tubes and placed on a thermomixer (Eppendorf, Germany) at 37 °C with the open lids until the solvents were completely evaporated. The residue was resuspended with 50 µL of EtOAc and subsequently analyzed using TLC, UV-illumination and Fe^{2+}/SCN staining.

Figure 3. Experimental setup for VLC. The loaded column was placed on a dripping funnel and connected to a vacuum pump. With the closed stop of the dripping funnel, each 20 mL of eluent mixture was placed on top of the column and elution was slowly initiated by vacuum. After most of the eluent has passed through the column and collected in the dripping funnel, the vacuum was disconnected and by opening the stop of the dripping funnel, the fraction was collected in 20 mL glass tubes. This was repeated 21 times.

Since UV-light illumination of TLC plates makes it hard to identify the produced EP, these were visualized by Fe^{2+}/SCN staining of the plates. Firstly, 120 mg of NH_4SCN and

NH_4FeSO_4 were weighed in Eppendorf tubes, separately. Afterwards, NH_4SCN was dissolved in 14 mL of acetone, while NH_4FeSO_4 was mixed with 1 mL of H_2O. The two solutions were mixed and 4 mL of the mixture was sprayed on the TLC plate and subsequently the plates were placed on hot plate at 95 °C. After 1 min of heating, the photos of the plates were taken.

The glass tubes, which contained fractions with the highest amount of desired product were evaporated using nitrogen and prepared for NMR analysis.

Table 2. VLC Fractions with the corresponding solvent mixture for each fraction.

Fraction number	Solvent 1	Vol 1 (mL)	Solvent 2	Vol 2 (mL)
	PE	20		
	PE	20		
	PE	20		
1	PE	20	EtOAc	0
2	PE	19	EtOAc	1
3	PE	18	EtOAc	2
4	PE	17	EtOAc	3
5	PE	16	EtOAc	4
6	PE	15	EtOAc	5
7	PE	14	EtOAc	6
8	PE	13	EtOAc	7
9	PE	12	EtOAc	8
10	PE	11	EtOAc	9
11	PE	10	EtOAc	10
12	PE	9	EtOAc	11
13	PE	8	EtOAc	12
14	PE	7	EtOAc	13
15	PE	6	EtOAc	14
16	PE	5	EtOAc	15
17	PE	4	EtOAc	16
18	PE	3	EtOAc	17
19	PE	2	EtOAc	18
20	PE	1	EtOAc	19
21	PE	0	EtOAc	20

2.6 Formation of the xylenol/Fe^{3+} complex by EP

Xylenol orange (XO) (125 μM) and butylated hydroxytoluene (BHT) (4 mM) were dissolved in 9:1 (v/v) MeOH/H_2O solution in order to create an organic peroxide reagent. $FeSO_4$ (25 mM)

was freshly dissolved in 2.5 M H_2SO_4. 25 mL of the organic peroxide reagent was mixed with 250 µL of the $FeSO_4$ solution to create the color reagent. 1 mL of the color reagent was mixed in a 1.5 mL cuvette (BRAND, Germany) with an aliquot of the analyzed compound to reach the final compound concentration of 100 µM. OD measurements at 1-minute intervals between 400 and 700 nm were performed for 20 minutes using a MS1501 UV-VIS diode array spectrophotometer (Shimadzu, Japan). MeOH/H_2O (9:1) was used as a reference. The wavelength of 560 nm was used for kinetic evaluation. The concentration change of EP due to the formation of radicals (Fe^{2+} conversion to Fe^{3+}) was calculated using the slope of the reaction and the extinction coefficient of the Fe^{3+}/XO complex: 15000 l * mol^{-1} * cm^{-1} (33).

2.7 Simulation of NMR spectra

Formulae of sterols and corresponding EP compounds were drawn in BIOVIA Draw 2021 (Dassault Systems) (Vélizy-Villacoublay, France) with explicit H display and exported as .mol files. For the prediction of NMR spectra, the tool "PREDICT ^{1}H NMR" on the website www.nmrdb.org was used (34). After the import of .mol files, simulation was started. The resulting spectra and formulae with H at the double bonds marked were saved by screenshots and used for further analysis (35, 36).

2.8 Experimental NMR

NMR spectra were recorded by Dr. Markus Bacher on a Bruker Avance II 400 (Rheinstetten, Germany) equipped with a 5 mm N_2-cooled cryo probe head (Prodigy) with z-gradients at room temperature. Resonance frequencies were 400.13 MHz for ^{1}H. Samples (ca. 20 mg) were dissolved in 0.6 mL $CDCl_3$ (99.8 % D). Chemical shifts are given in δ ppm values, referenced to residual solvent signal ($CDCl_3$, 7.26 ppm for ^{1}H). The resulting NMR spectra were analyzed using TopSpin 3.6.4 (Bruker) software. For evaluation of ErgoEP sample purity following signal integrals were used at (δ): 6.57, 6.48 and 5.56 for DHErgoEP, ErgoEP and Ergo, respectively. For DHCholEP samples following signal integrals were used at (δ): 6.60, 6.50, and 5.57 for TDHChol, DHCholEP and DHChol, respectively. Integrals were summed up, set as 100 % and respective portions of compounds were expressed in percent.

3. Results

3.1 Basic ^{1}H NMR spectra prediction

In order to understand the experimental NMR spectra of our synthetic products, NMR simulations were performed to identify the peaks corresponding to the hydrogens that are changed by oxygen addition during the photo-oxidation process. In particular, the focus was on the yellow-marked hydrogens bound to C6 and C7 (Figure 4). The data acquired from the simulations suggest that the cycloaddition of oxygen at the 5,8-position of Ergo causes H-7 and H-8 to resonate at a higher frequency, causing a positive δ chemical shift (Figure 4, 6). The same pattern was observed for DHChol and DHCholEP, respectively (Figure 5, 7).

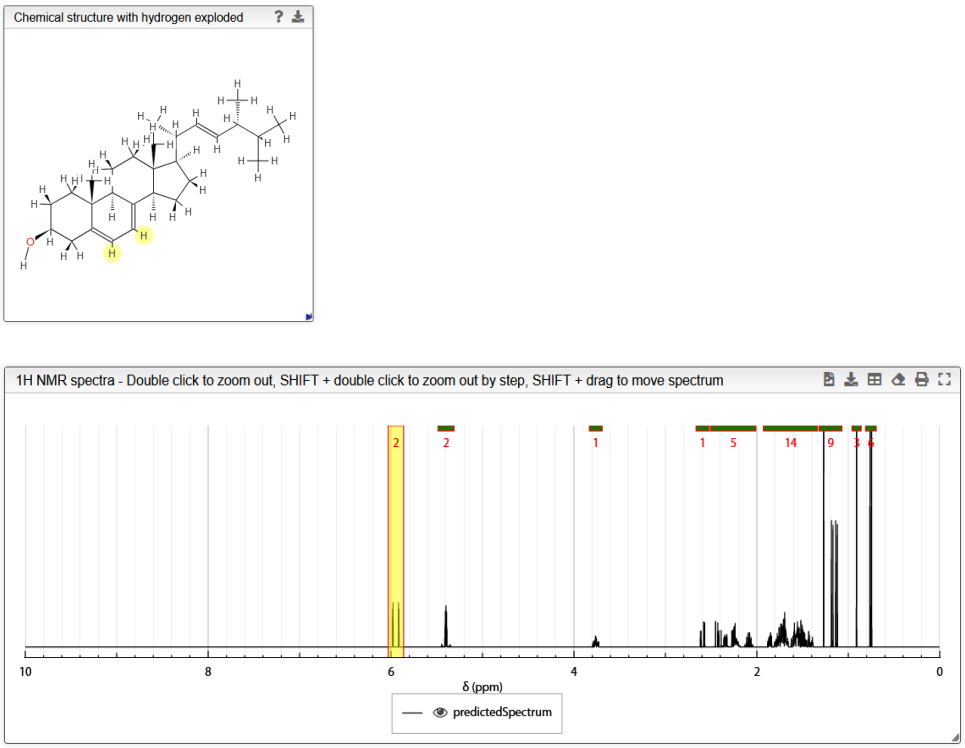

Figure 4. Simulated ^{1}H NMR spectrum of Ergo. Upper graph shows molecular structure of Ergo used for simulation. Lower graph shows the simulated ^{1}H NMR spectrum. Atoms and peaks highlighted in yellow are expected to change their chemical shift during photo-oxidation. Resonance of H at the ring double bonds were predicted at δ 5.915 and 5.979.

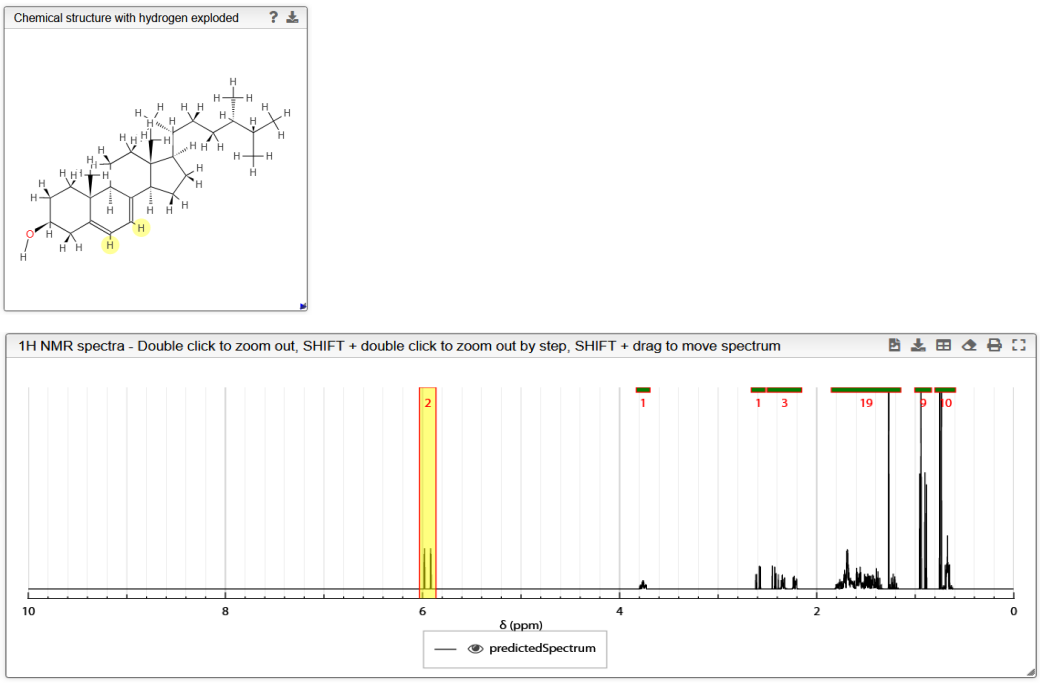

Figure 5. Simulated ^{1}H NMR spectrum of DHChol. Upper graph shows molecular structure of DHChol used for simulation. Lower graph shows the simulated ^{1}H NMR spectrum. Atoms and peaks highlighted in yellow are expected to change their chemical shift during photo-oxidation. Resonance of H at the ring double bonds were predicted at δ 5.915 and 5.979.

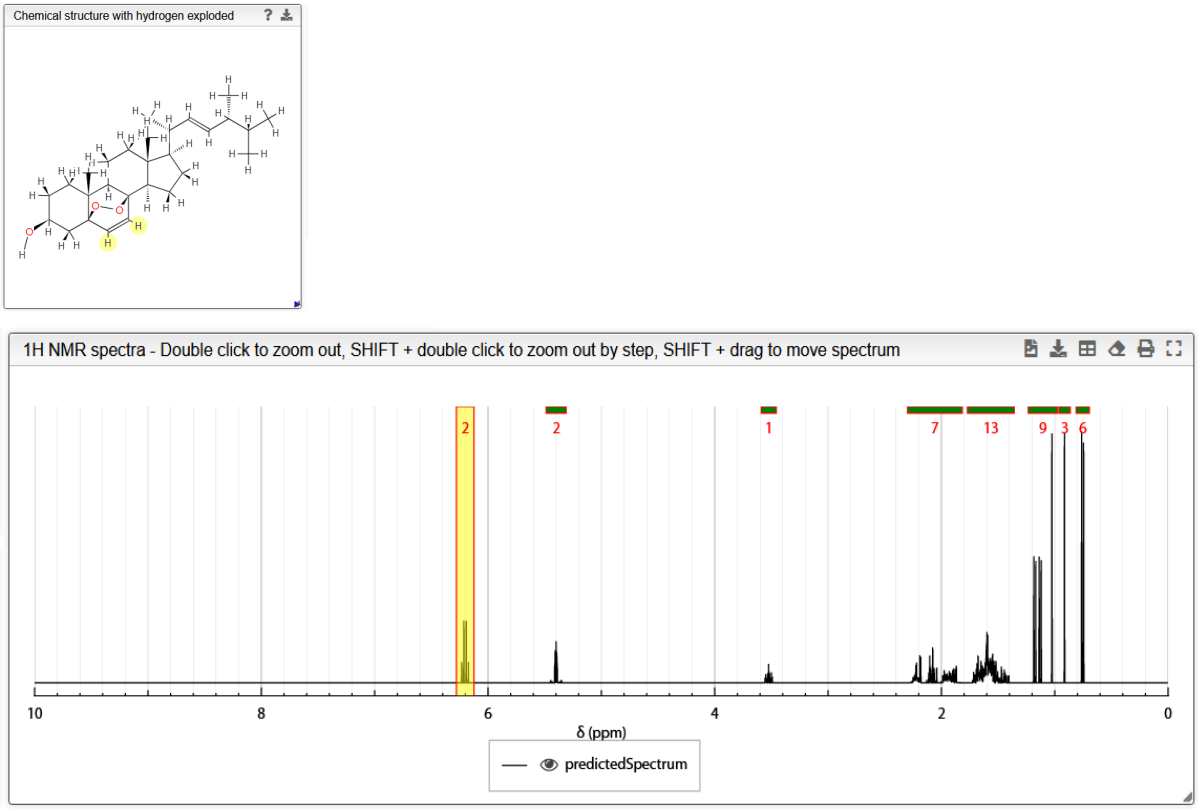

Figure 6. Simulated ^{1}H NMR spectrum of ErgoEP. Upper graph shows molecular structure of ErgoEP used for simulation. Lower graph shows the simulated ^{1}H NMR spectrum. Atoms and peaks highlighted in yellow have changed their chemical shift during photo-oxidation. Resonance of H at the ring double bonds were predicted at δ 6.184 and 6.219.

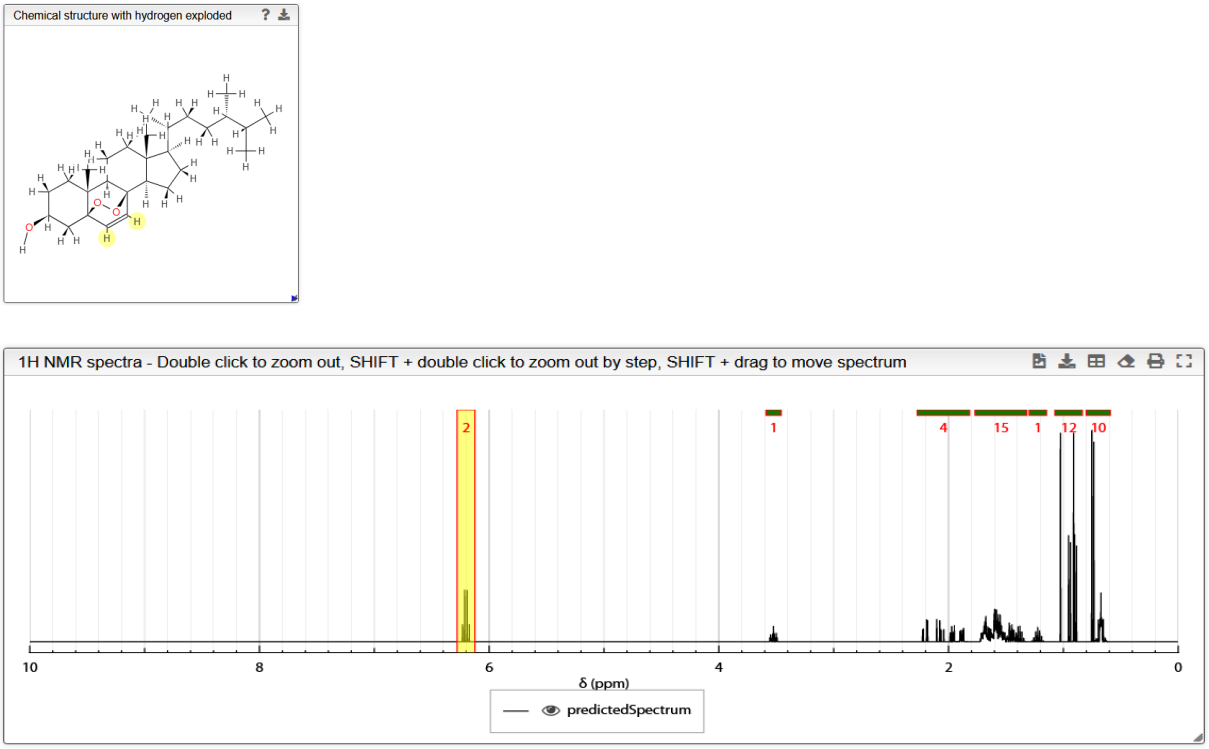

Figure 7. Simulated ^{1}H NMR spectrum of DHCholEP. Upper graph shows molecular structure of DHCholEP used for simulation. Lower graph shows the simulated ^{1}H NMR spectrum. Atoms and peaks highlighted in yellow have changed their chemical shift during photo-oxidation. Resonance of H at the ring double bonds were predicted at δ 6.184 and 6.219.

It is expected that the synthesis of sterol EP through the photo-oxidation method leads to the formation of side products as well. Possible side products are created through an additional dehydrogenation process at C9 position, leading to the formation of dehydroergosterol peroxide (DHErgoEP) and tetra-dehydrocholesterol peroxide (TDHCholEP). NMR simulation was performed for these molecules as well (Figure 8, 9). According to the simulation, this additional dehydrogenation process causes further positive δ chemical shift of our targeted hydrogens, in comparison with ErgoEP and DHCholEP.

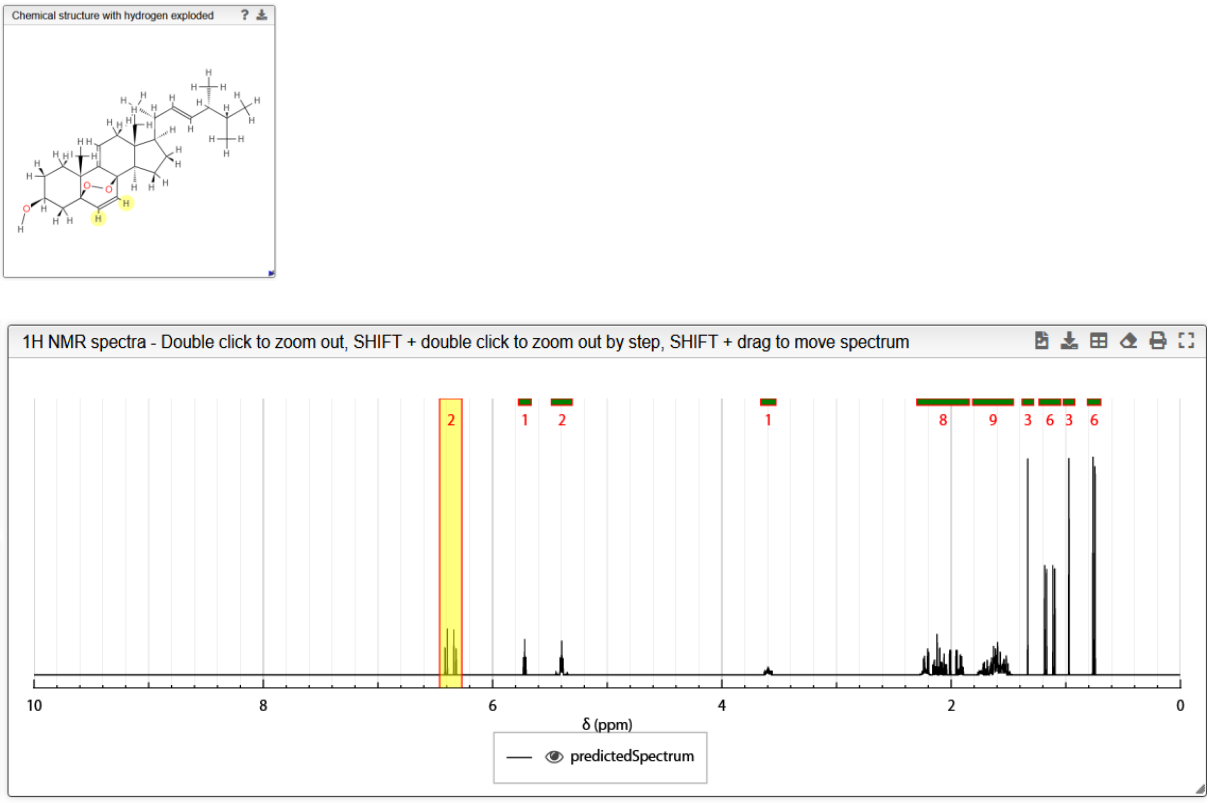

Figure 8. Simulated ^{1}H NMR spectrum of DHErgoEP. Upper graph shows molecular structure of DHErgoEP used for simulation. Lower graph shows the simulated ^{1}H NMR spectrum. Atoms and peaks highlighted in yellow have changed their chemical shift during photo-oxidation. Resonance of H at the ring double bonds were predicted at δ 6.328 and 6.402.

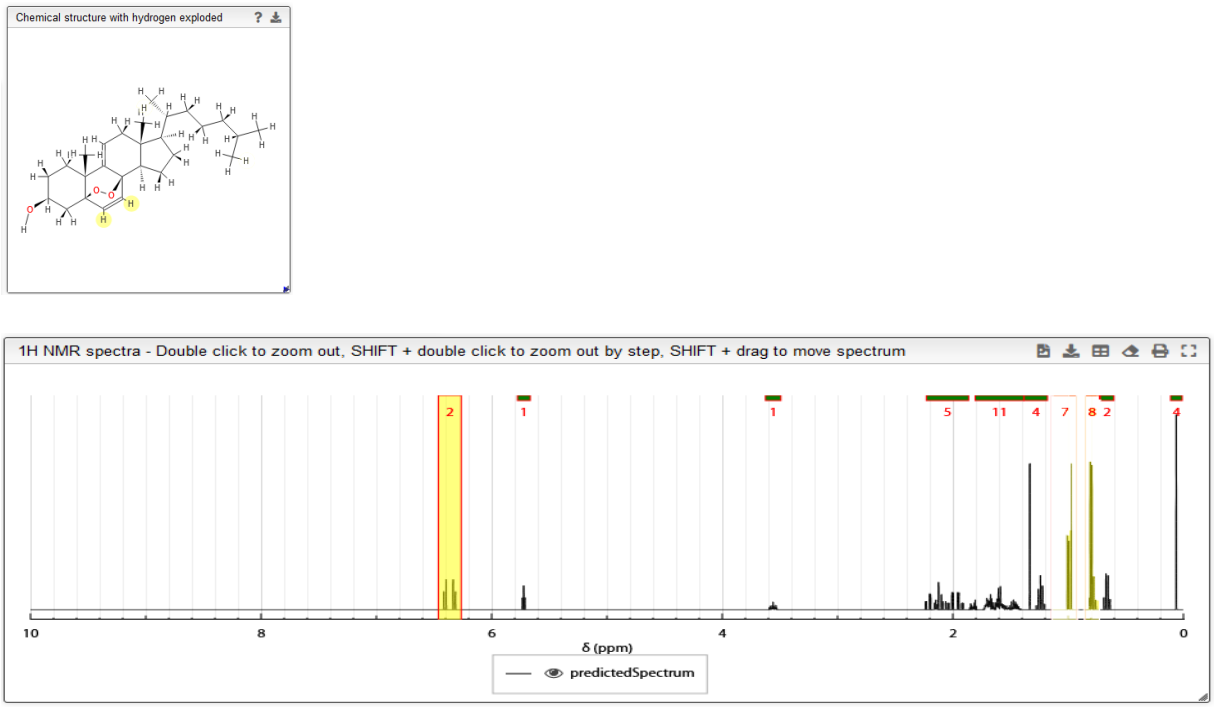

Figure 9. Simulated ^{1}H NMR spectrum of TDHCholEP. Upper graph shows molecular structure of DHErgoEP used for simulation. Lower graph shows the simulated ^{1}H NMR spectrum. Atoms and peaks highlighted in yellow have changed their chemical shift during photo-oxidation. Resonance of H at the ring double bonds were predicted at δ 6.328 and 6.402.

3.2 Synthesis

Figure 10 shows the reactions leading to the formation of sterol EP through photo-oxidation. In addition, for Ergo and DHChol, there is a possibility of an additional oxidation process through dehydrogenation at C9, leading to the formation of DHErgoEP and TDHCholEP, respectively (Figure 11). The main goal was to develop a synthetic method that can minimize the concentration of side products in the sample. During the synthetic processes, different PS, solvent and irradiation time combinations were used (Table 3).

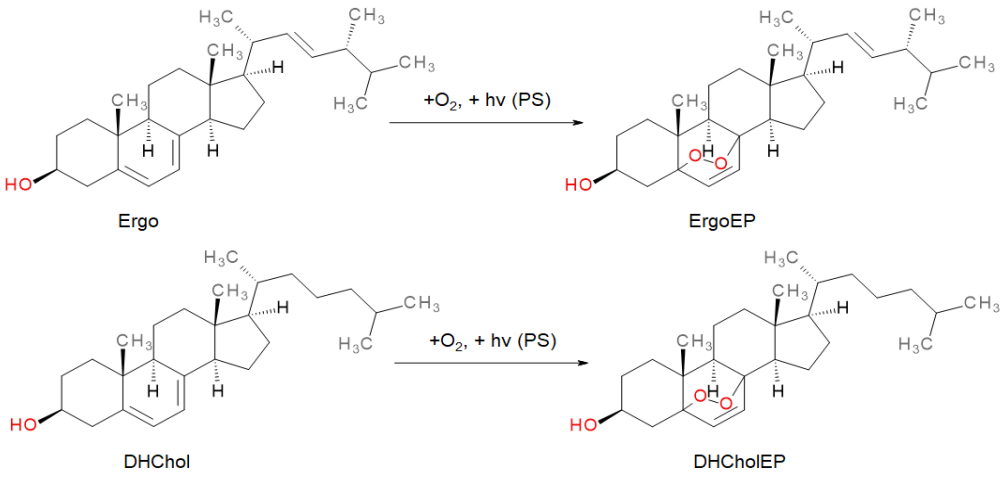

Figure 10. Reaction scheme of photo-oxidation of Ergo and DHChol to their corresponding EP. Upper reaction equation shows the transformation of Ergo to ErgoEP via photo-oxidation, in the presence of oxygen, light energy and photosensitizer (PS). Lower reaction equation shows the same transformational process of DHChol to DHCholEP.

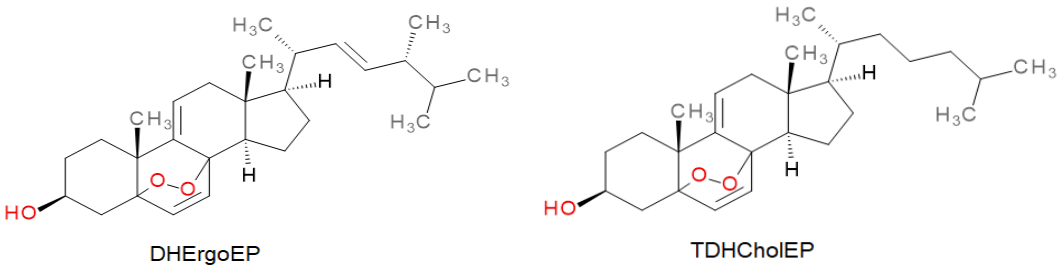

Figure 11. Possible side products of photo-oxidation of sterols. In comparison to ErgoEP and DHCholEP, there is an additional double bond at 9,10-position. On the left side: dehydroergosterol peroxide (DHErgoEP), on the right side: tetra-dehydrocholesterol peroxide (TDHCholEP). It is expected that these products are formed by an additional dehydrogenation process during photo-oxidation.

Table 3. Variants of synthesis performed for photo-oxidation of sterols. Table shows different synthetic variants, with the type and amount of sterol which was used, type and amount of photosensitizer (PS), the used solvent for the reaction and the reaction time. As for the reaction time, the time of the irradiation with tungsten filament light is considered. PS used are methylene blue (MB) and Eosin Y (EY).

Variant	Sterol	PS	Solvent	Time
V1	Ergo 200 mg	MB 5 mg	CH_2Cl_2	20 min
V2	Ergo 200 mg	EY 3 mg	EtOH	60 min
V3	DHChol 200 mg	MB 5 mg	CH_2Cl_2	20 min
V4	DHChol 200 mg	EY 3 mg	EtOH	60 min

3.3 Reaction monitoring

An example of TLC monitoring of synthetic reaction is shown in Figure 12. During the synthetic process, several samples at different time intervals were taken for the TLC analysis (Table 4). The presence of the dark violet spot under UV light indicates the presence of the educts, DHChol or Ergo (Figure 12, 13). The educt presented in figure 12 is Ergo. In lanes 4 and 5, the dark violet spot disappears due to the consumption of Ergo and production of sterol EP. The same pattern can be observed during the DHChol photooxidation process (Figure 13). From the literature the Rf values for Ergo and its corresponding peroxide were predicted in this solvent system to be 0.4 and 0.23, respectively (42). On our TLC plates, we detected Ergo at an Rf value of 0.38–0.39 (Figure 12). TLC chromatograms of all batches from one compound/photosensitizer combination were similar. Therefore, we display only typical examples of TLC chromatograms.

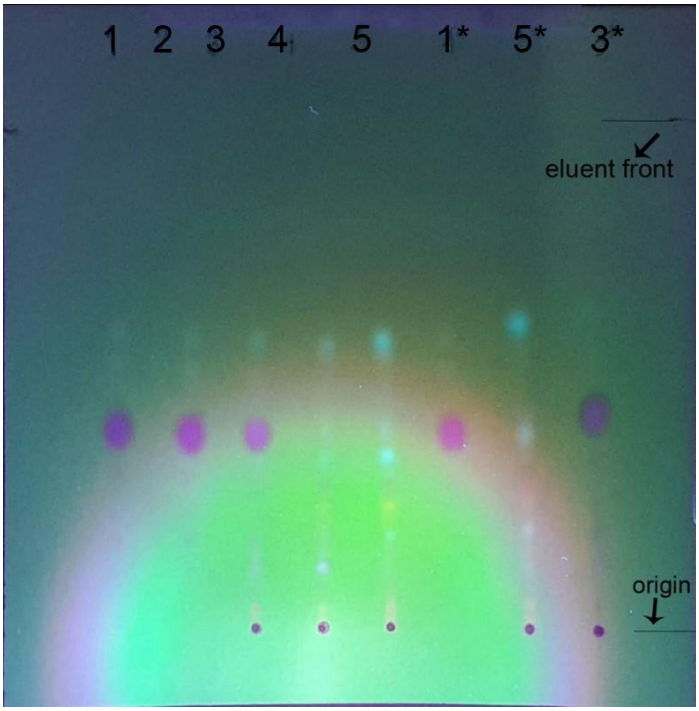

Figure 12. Typical TLC plate of the reaction of Ergo with O_2 in the presence of MB visualized by UV illumination. $CHCl_3$/MeOH (3 % v/v) solution was used as eluent. The content of each lane is described in Table 4 (instead of DHChol, Ergo was used). Lanes 1*, 3* and 5* are duplicates of respective lanes. Dark violet spots above origin in lanes 1-3 represent Ergo. Rf values of Ergo: lane 1: 0.39, lane 2: 0.38, lane 3: 0.38. Reference Rf of Ergo is 0.4. Small violet spots at the origin in lanes 3-5 represent the photosensitizer MB, because it does not migrate in this solvent system. Other spots are of unknown origin.

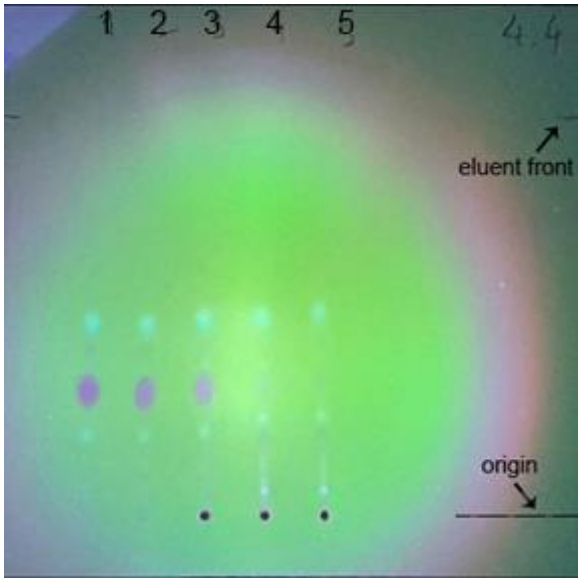

Figure 13. Typical TLC plate of the reaction of DHChol with O_2 in the presence of MB visualized by UV illumination. $CHCl_3$/MeOH (3 % v/v) solution was used as eluent. The content of each lane is described in Table 4. Dark violet spots above origin in lanes 1-3 represent DHChol. Retention factor (Rf) values of DHChol: lane 1: 0.34, lane 2: 0.33, lane 3: 0.37. Small violet spots at the origin in lanes 3-5 represent the photosensitizer MB, because it does not migrate in this assay. Other spots are of unknown origin.

Table 4. Typical example of the samples taken for the TLC analysis during the DHCholEP synthetic process.

Lane	Sample	Description
1	S1	DHChol
2	S2	DHChol after one 1 h of O_2 flow
3	S3	DHChol 5 minutes after the addition of MB/EY
4	S4	DHChol after 10/30 min of the irradiation time with tungsten filament light
5	S5	DHChol after the irradiation with tungsten filament light

After the VLC separation of EP, each fraction was analyzed using TLC as well. The absence of DHChol in the fractions was confirmed under the UV light (Figure 14). EP can not be detected under the UV light, thus, the Fe^{2+}/SCN staining of the plates was applied (Figures

15, 16). The spots with some tailing and trailing indicate the presence of EP. Fe^{2+}/SCN staining demonstrated that major portions of EP were in fractions 13 and 14, so we decided to study these fractions by NMR.

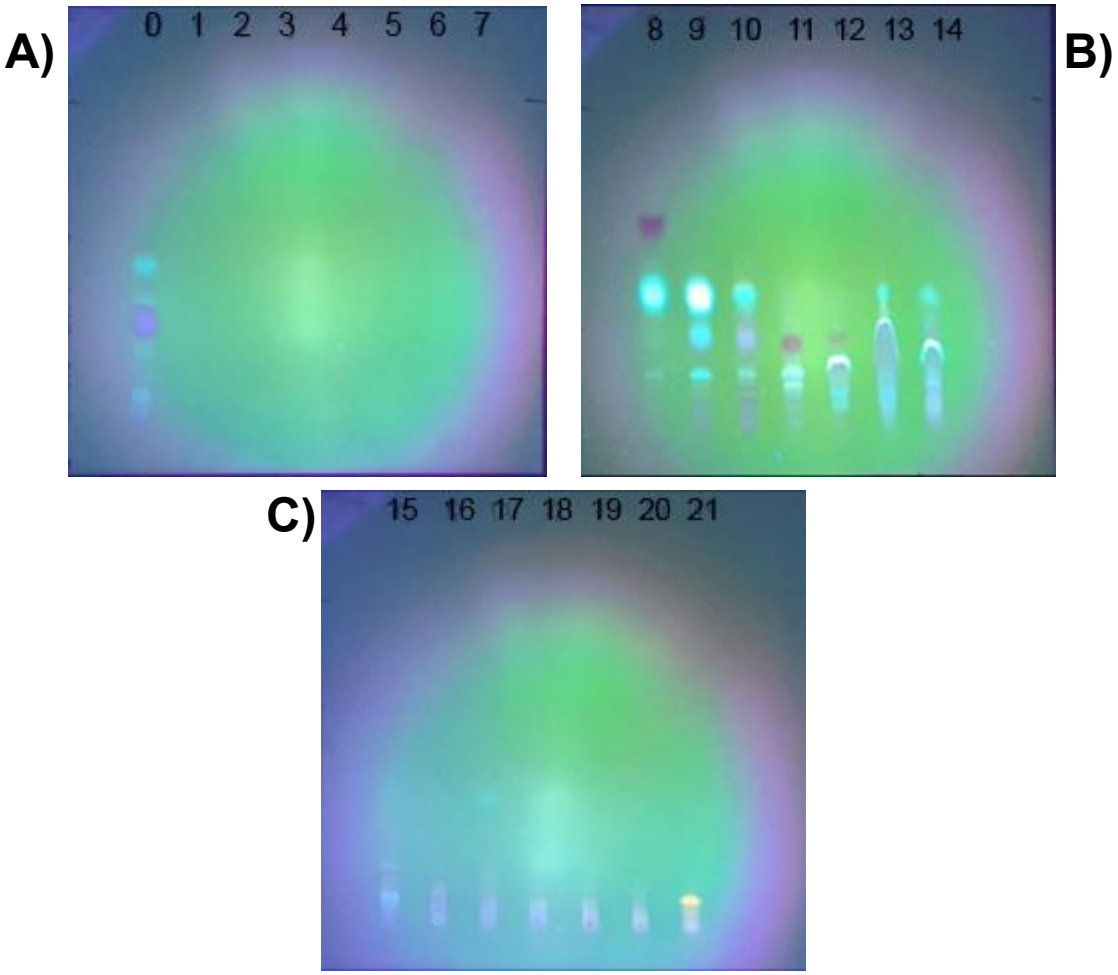

Figure 14. Typical TLC plate of fractions obtained by VLC purification of reaction products of DHChol with O_2 in the presence of MB visualized by UV illumination. $CHCl_3$/MeOH (3 % v/v) solution was used as eluent during TLC. Handwritten numbers above lanes correspond to fraction numbers. Composition of VLC eluent in each fraction was described in the "Materials and methods" section (Table 2). Figure shows fractions 1-21, while lane 0 contains 5 µL of 40 mM DHChol as control. Dark violet spot in lane 0 represents DHChol, while other spots are of unknown origin. Rf value of DHChol in lane 0 is 0.32.

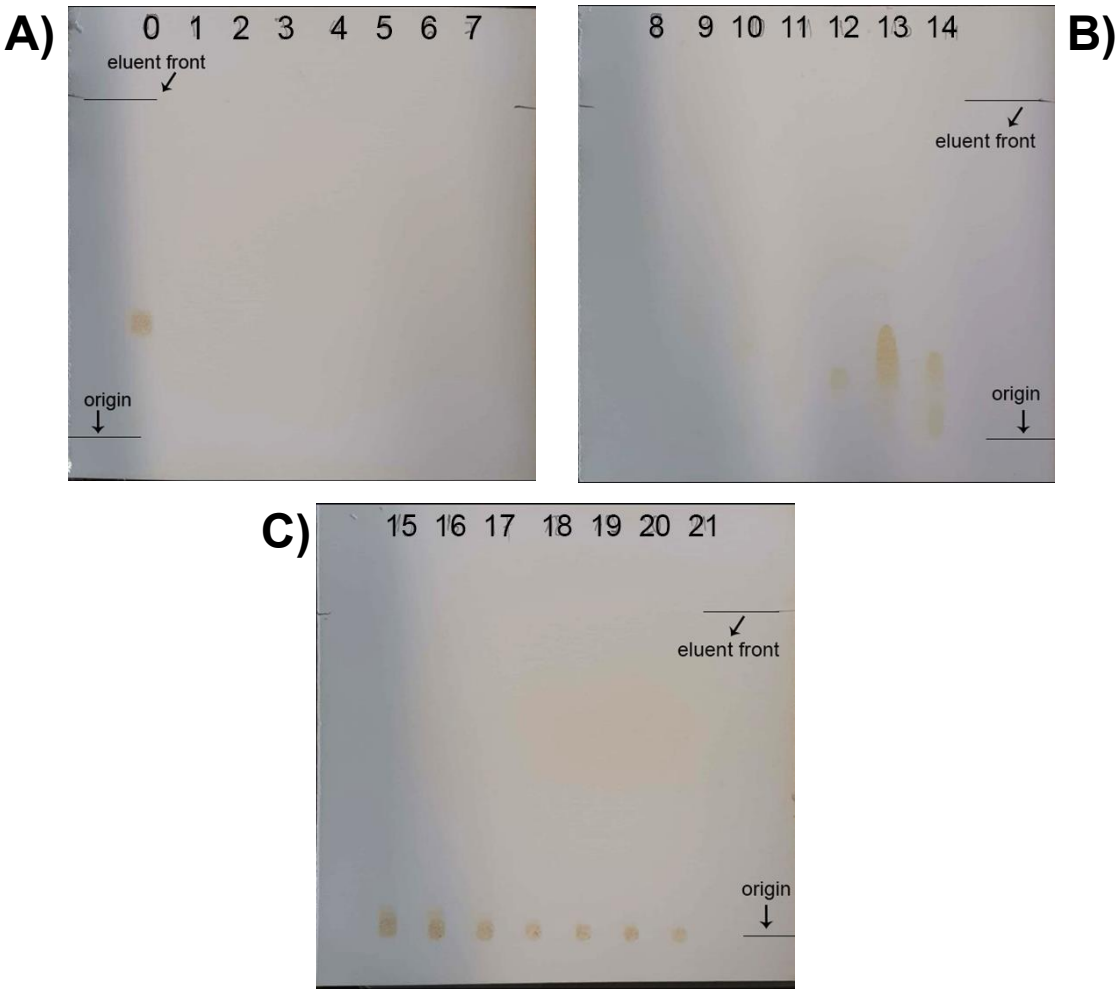

Figure 15. Typical TLC plate of fractions obtained by VLC purification of reaction products of DHChol with O_2 in the presence of MB visualized by Fe^{2+}/SCN staining. $CHCl_3$/MeOH (3 % v/v) solution was used as eluent. Composition of VLC eluent in each fraction was described in "Materials and methods" section (Table 2). Figure shows fractions 1-21, while lane 0 contains 5 µL of 40 mM DHChol as control. Orange spot in lane 0 represents DHChol, spots in lanes 12, 13 and 14 show the presence of DHCholEP. Rf values of DHCholEP: lane 13: 0.23, lane 14: 0.21. Spot in lane 12 was of insufficient intensity, therefore the Rf value was not measured.

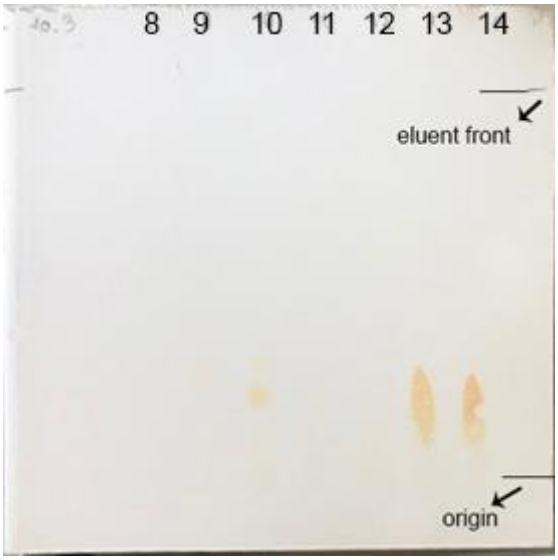

Figure 16. Typical TLC plate of fractions 8-14 obtained by VLC purification of reaction products of Ergo with O_2 in the presence of MB visualized by Fe^{2+}/SCN staining. $CHCl_3$/MeOH (3 % v/v) solution was used as eluent. Composition of VLC eluent in each fraction was described in "Materials and methods" section (Table 2). The spots in lanes 13 and 14 show the presence of ErgoEP. Rf values of ErgoEP: lane 13: 0.21, lane 14: 0.2. Reference Rf of ErgoEP: 0.23.

3.4 ^{1}H NMR of educts and products

To understand the NMR spectra of products, the experimental ^{1}H NMR spectra of educts (Ergo, DHChol) were acquired (Figure 17, 18). Comparing the observed spectra with the obtained simulated data, the δ chemical shifts of the H at the ring double bonds of the educts were extracted (Table 5). The experimental data match the results from the simulated data. This suggests that the cycloaddition of oxygen at the 5,8-position of sterols causes targeted hydrogens to resonate at a higher frequency, causing a positive δ chemical shift. In the case of Ergo, the experimental δ chemical shifts (5.38/5.56) are lower than the simulation values (5.91/5.97). Same pattern can be observed with DHChol, with experimental δ being 5.38/5.57 and calculated at δ 5.91/5.97.

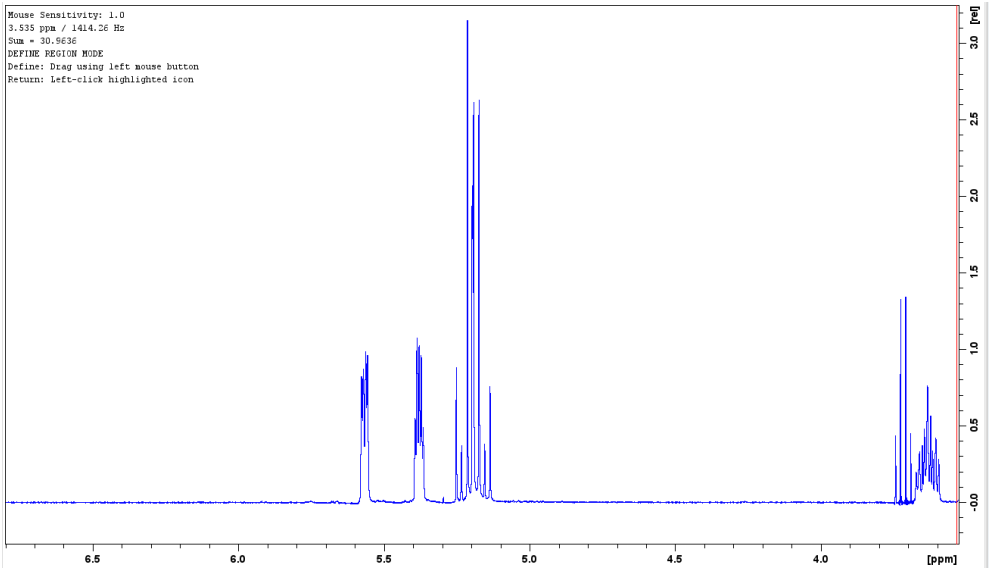

Figure 17. Experimental ^{1}H NMR spectrum of Ergo. Region of the spectra between δ 4 and 6.5 ppm is displayed. About 20 mg of Ergo was dissolved in $CDCl_3$.

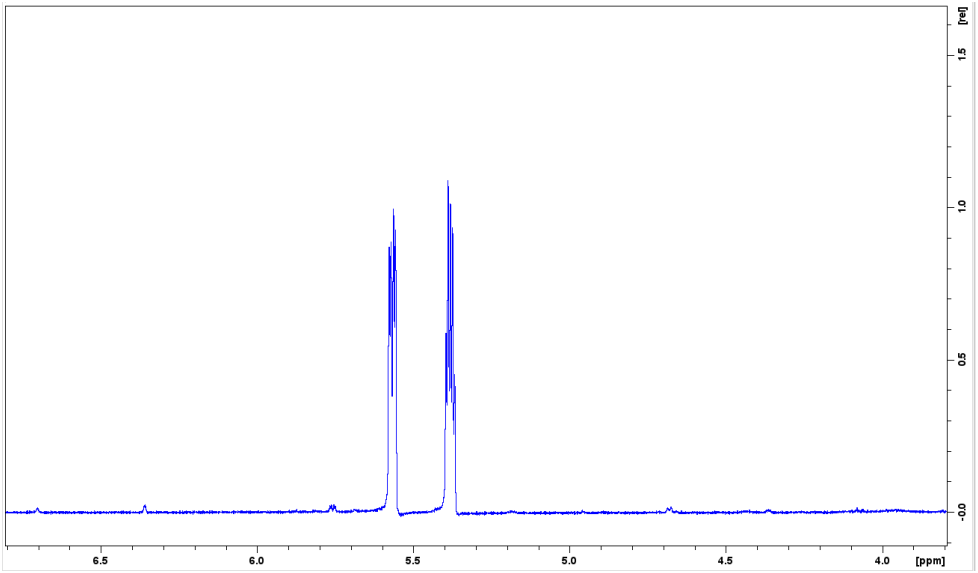

Figure 18. Experimental ^{1}H NMR spectrum of DHChol. Region of the spectra between δ 4 and 6.5 ppm is displayed. About 20 mg of DHChol was dissolved in $CDCl_3$.

Knowing the experimental δ values of the educts, the NMR-spectra of the purified products of Ergo and DHChol photo-oxidation were analyzed. The peaks corresponding to the H at the targeted double bond of educts, products and side products were identified by comparing the simulated shifts with the experimental ^{1}H NMR spectrum of a purified product of the photo-oxidation (Figure 19, 20). For evaluation of ErgoEP sample purity following signal integrals

were used at (δ): 6.57, 6.48 and 5.56 for DHErgoEP, ErgoEP and Ergo, respectively. For DHCholEP samples following signal integrals were used at (δ): 6.60, 6.50, and 5.57 for TDHChol, DHCholEP and DHChol, respectively. Sample purity was measured and displayed in percent for each individual fraction (Table 6, 7). The samples with the highest yield and purity were taken for further work (220301_Ergo_MB_F14 in case of ErgoEP, and 220331_DHCholEP_MB_F13 for DHCholEP).

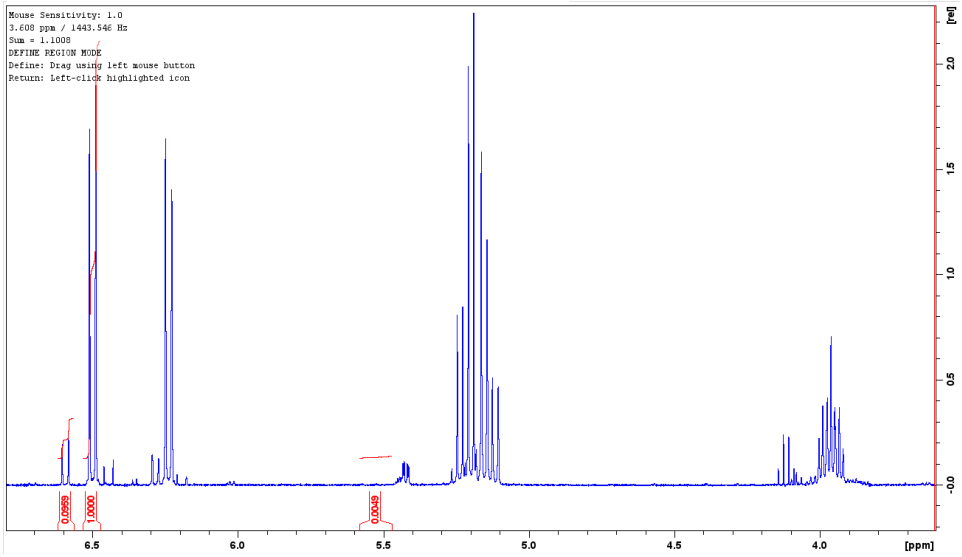

Figure 19. Experimental ^{1}H NMR spectrum of a purified product of Ergo photo-oxidation. Region of the spectra between δ 4 and 7 ppm is displayed. About 20 mg of the product was dissolved in $CDCl_3$. The signal integrals (marked in red) at (δ): 6.57 (DHErgoEP), 6.48 (ErgoEP) and 5.56 (Ergo) were used for calculating the purity of the obtained product fraction.

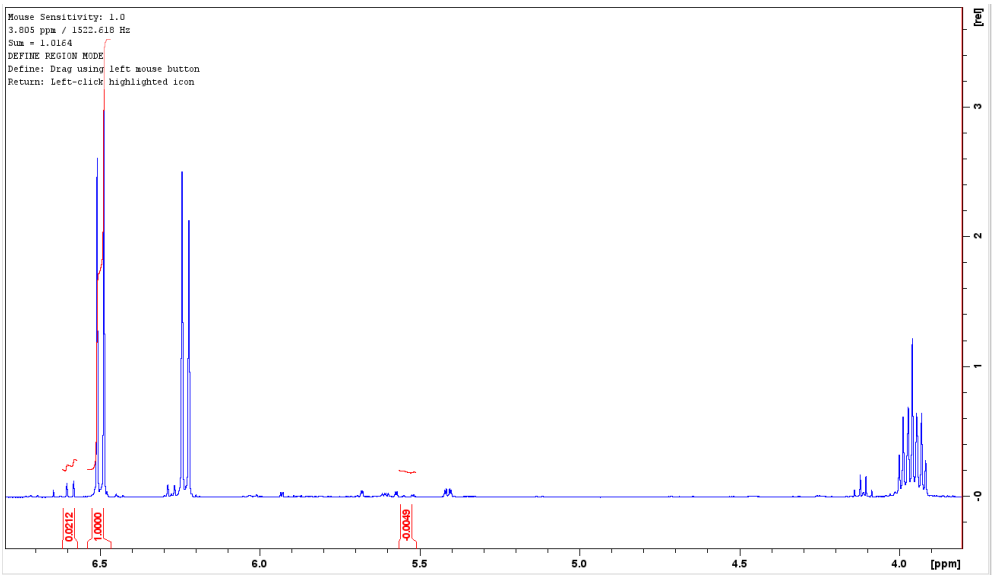

Figure 20. Experimental ^{1}H NMR spectrum of a purified product of DHChol photo-oxydation. Region of the spectra between δ 4 and 7 ppm is displayed. About 20 mg of the product was dissolved in $CDCl_3$. The signal integrals (marked in red) at (δ): 6.60 (TDHCholEP), 6.50 (DHCholEP) and 5.57 (DHChol) were used for calculating the purity of the obtained product fraction.

Table 5. ^{1}H NMR shifts of H at ring double bonds in sterols and corresponding EP.

Compound	Predicted Shifts (δ)	Experimental Shifts (δ)
Ergo	5.91/5.97	5.38/5.56
ErgoEP	6.18/6.21	6.20/6.48
DHErgoEP	6.32/6.40	6.26/6.57
DHChol	5.91/5.97	5.38/5.57
DHCholEP	6.18/6.21	6.24/6.50
TDHChol	6.32/6.40	6.28/6.60

Table 6. Purity and amount of synthesized fractions from Ergo. Synthesis variants have been described in table 3.

Internal Name	Synthesis Variant	Fraction	Amount (mg)	ErgoEP (%)	DHErgoEP (%)	Ergo (%)
220301_Ergo_MB_F13	V1	F13	172	67.6	30.1	2.2
220301_Ergo_MB_F14	V1	F14	230	90.2	9.4	0.3
220316_Ergo_EY_F13	V2	F13	128	85.7	14.3	0.02
220316_Ergo_EY_F14	V2	F14	68	91.2	8.7	0.3

Table 7. Purity and amount of synthesized fractions from DHChol. Synthesis variants have been described in table 3.

Internal Name	Synthesis Variant	Fraction	Amount (mg)	DHCholEP (%)	TDHCholEP (%)	DHChol (%)
220331_DHCholEP_MB_F13	V3	F13	249	95.9	3.0	1.0
220412_DHCholEP_EY_F13	V4	F13	240	86.5	12.2	1.3
220412_DHCholEP_EY_F14	V4	F14	85	96.2	2.0	1.8

3.5 Viability

The influence of ErgoEP and DHCholEP and the corresponding educts on the viability of LtP was studied. Typical examples of viability/concentration curves derived from resazurin viability assays for both vertical and horizontal concentration gradients are shown in figures 21 and 22. These curves were used to calculate the IC_{50} values of each compound. It is shown in tables 8 and 9, that the IC_{50} values of sterol EP are lower compared to their respective educts, and DHCholEP seems to be more toxic for LtP compared to ErgoEP.

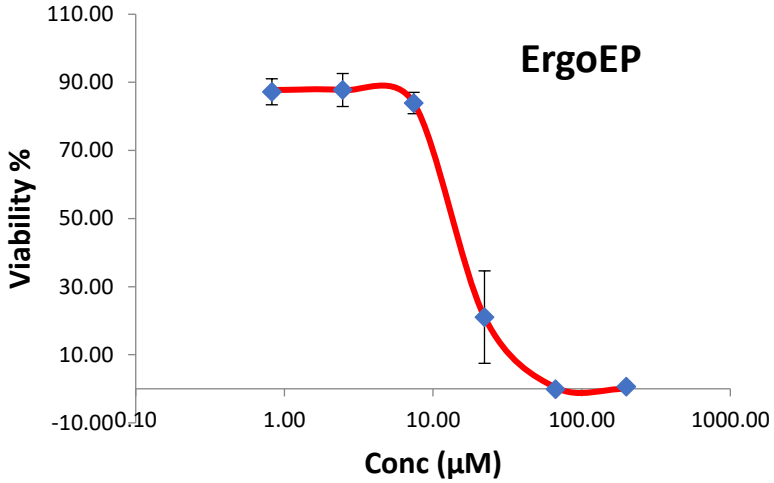

Figure 21. Typical viability-concentration curve for LtP as a function of different concentrations of ErgoEP (0.097 µM to 200 µM) in 96-well plates with vertical concentration gradients. The IC_{50} value obtained from this experiment was 16.50 ± 0.18 µM for ErgoEP. Individual data points represent mean ± SD of triplicate measurements.

Table 8. Influence of sterols (Ergo, DHChol) and corresponding peroxides (ErgoEP, DHCholEP) on the viability of LtP in 96-well plates with vertical concentration gradients (6 concentrations). Substances were tested in the concentration range from 0.097 µM to 200 µM. The IC_{50} values were determined using resazurin viability assays with the substances dissolved in EtOH (20 mM stocks) with an endpoint of 48 h and starting with $2*10^6$ LtP/ml. Data represent mean ± SD of 4-5 plates.

Compound	LtP IC_{50} (µM) Mean ± SD
Ergo	30.98 ± 16.47
ErgoEP	12.38 ± 4.98
DHChol	9.63 ± 1.20
DHCholEP	5.22 ± 2.19

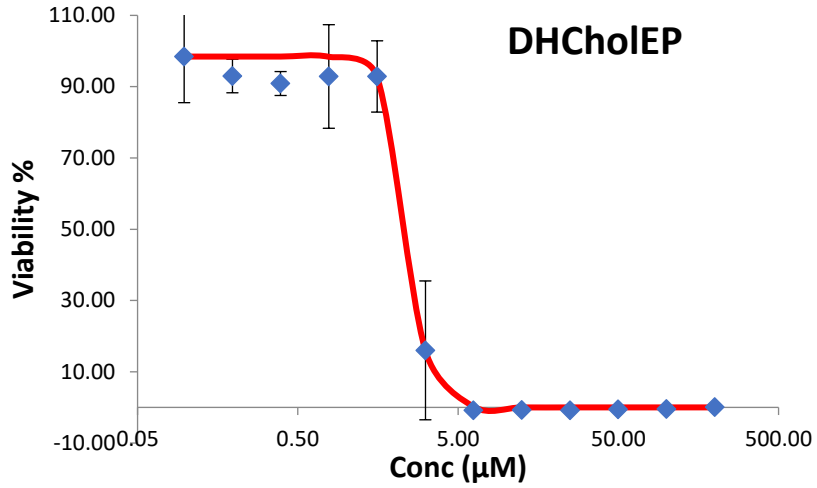

Figure 22. Typical viability-concentration curve for LtP as a function of different concentrations of DHCholEP (0.082 µM to 200 µM) in 96-well plates with horizontal concentration gradients. The IC_{50} value obtained from this experiment was 2.41 ± 0.11 µM for DHCholEP. Individual data points represent mean ± SD of duplicate measurements.

Table 9. Influence of sterols (Ergo, DHChol), corresponding peroxides (ErgoEP, DHCholEP) and reference compounds (Pen, Chol) on the viability of LtP in 96-well plates with horizontal concentration gradients (12 concentrations). Substances were tested in the concentration range from 0.082 µM to 200 µM and 0.01 µM to 20 µM for Pen. The IC_{50} values were determined using resazurin viability assays with the substances dissolved in EtOH (20 or 5 (Pen) mM stocks) with an endpoint of 48 h and starting with $2*10^6$ LtP/ml. Data represent mean ± SD of 4-5 plates.

Compound	LtP IC_{50} (µM) Mean ± SD
Ergo	12.07 ± 6.53
ErgoEP	6.65 ± 5.63
DHChol	7.45 ± 5.52
DHCholEP	2.16 ± 0.30
Chol	> 200
Pen	1.38 ± 0.95

The mechanism of action of certain EP against *Leishmania* is mediated by the formation of carbon-centered radicals that can cause antileishmanial properties. Therefore, introducing a radical scavenger, such as NAC, in the viability assay procedure should prevent the antileishmanial effects of these substances, and increase the IC_{50} values. The viability-concentration curves of the EP with and without the addition of NAC were compared (Figure 23). Considering both curves, there is a slight curve shift towards higher concentration values after the addition of NAC. Table 10 shows that there is a tendency of increase in IC_{50} values of Ergo, ErgoEP, DHChol and DHCholEP following the addition of NAC. These observations indicate that the mechanism of action of sterol EP could partially involve radical formation.

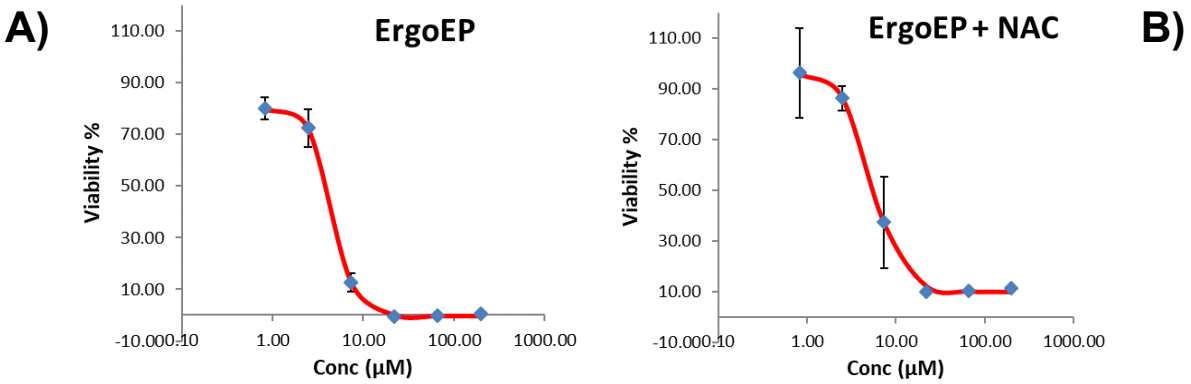

Figure 23. Typical viability-concentration curves for LtP as a function of different concentrations of ErgoEP without (left) and with (right) the addition of 2 mM NAC to the media. The IC_{50} values obtained from this experiment were 4.65 ± 0.04 µM for ErgoEP and 5.46 ± 0.14 µM for ErgoEP with 2 mM NAC. The resulting change in this case was calculated to be 117 %. Individual data points represent mean ± SD of triplicate measurements.

Table 10. Influence of NAC (2 mM) on IC_{50} values of sterols and corresponding peroxides on the viability of LtP in 96-well plates with vertical concentration gradients (6 concentrations). Substances were tested in the concentration range from 0.82 µM to 200 µM. The IC_{50} values were determined using resazurin viability assays with the substances dissolved in EtOH (20 mM stocks) with an endpoint of 48 h and starting with $2*10^6$ LtP/ml. Data represent mean ± SD of 3-4 plates. Relative IC_{50} values have been obtained by dividing the IC_{50} of a compound treated with NAC, through original IC_{50} of a compound. This has been repeated for all replicates. Afterwards, the mean and standard deviation of the replicates were multiplied by 100 (%). The original IC_{50} was set to 100%.

Compound	LtP + NAC Relative IC_{50} (%) Mean ± SD
Ergo	122 ± 55
ErgoEP_0301	122 ± 19
DHChol	163 ± 71
DHCholEP_0331	112 ± 37

3.6 Reaction of EP with Fe^{2+}

EP like Asc tend to react with Fe^{2+} leading to the radical formation, which is a requirement for their cytotoxic capabilities (9). The resulting oxidized form Fe^{3+} forms a complex with XO which can be photometrically detected and kinetically evaluated at 560 nm (Figure 24). The formation rate of the Fe^{3+}/XO complex is, therefore, equivalent to the conversion rate of EP to radicals. This reaction was used to determine if the antileishmanial properties of sterol EP are triggered through a reaction with Fe^{2+}. Table 11 shows conversion rates for sterols and corresponding EP. Asc was used as a positive control substance, while Chol was used as a negative control. Interestingly, both sterols and EP reacted with Fe^{2+}, with the exception of Chol.

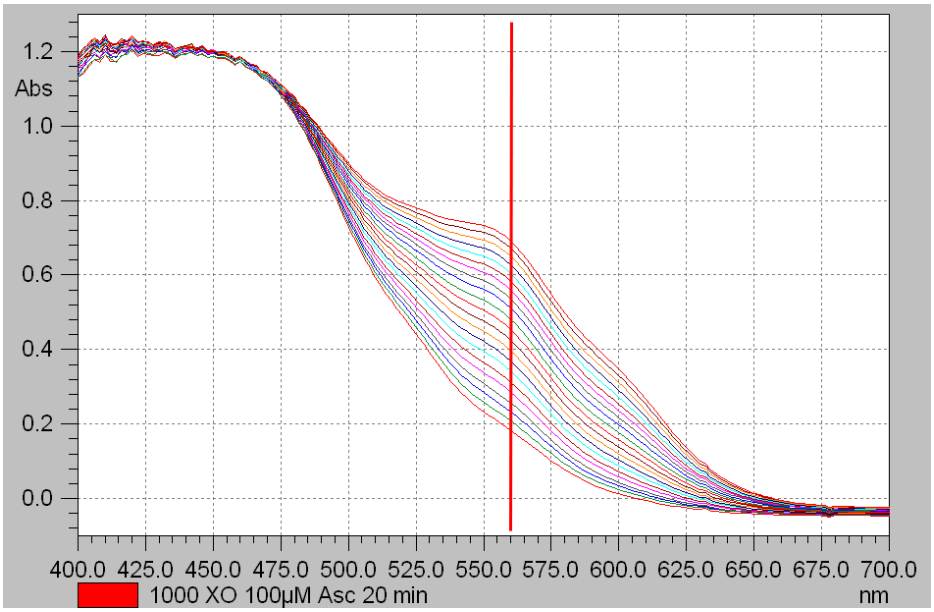

Figure 24. Visual spectra of the formation (lowest trace at t = 0 s, time interval = 1 min) of the Fe^{3+}/XO complex from the reaction of Asc (100 µM) with Fe^{2+} (250 µM) dissolved in MeOH/H_2O (9:1) in the presence of XO and air. The wavelength of 560 nm (red line) was used for kinetic evaluation.

Table 11. Formation rates of the Fe^{3+}/XO complex. The OD increase at 560 nm over time was determined using a spectrophotometer. MeOH/H_2O (9:1) was used as reference. Data represent mean ± SD of 3 experiments. For the biphasic behavior in the case of sterols, the slope of the initial increase was measured as Phase 1 and the slow increase afterwards as Phase 2.

Compound	Fe^{3+}/XO Formation Phase 1 (nmol/min) Mean ± SD	Fe^{3+}/XO Formation Phase 2 (nmol/min) Mean ± SD
Asc	106 ± 16	
Ergo	536 ± 148	17 ± 2
ErgoEP	208 ± 112	23 ± 4
DHChol	418 ± 11	21 ± 5
DHCholEP	169 ± 38	23 ± 1
Chol	4 ± 2	

4. Discussion

Leishmaniasis is a persistent and expanding global health problem. The endemic areas of this disease strongly depend on the distribution of the insect vector (sandflies). Due to climate change, endemic areas of the parasite vector expand to new regions, also in Europe (1).

The leishmaniasis disease is caused by a variety of protozoal parasite species from the genus *Leishmania*, which can lead to very different clinical manifestations and strongly depend on the region of the world where they occur. This multitude of *Leishmania* species and clinical manifestations makes pharmacological therapy difficult. In addition, antimonials used for several decades to combat visceral leishmaniasis in India are compromised by increasingly resistant *Leishmania* strains. Furthermore, depending on the region of the world and the endemic *Leishmania* species, different drugs are approved in different countries, such as Pen, amphotericin B, miltefosine. Therefore, availability and costs of these drugs in other parts of the world partially prevent their extensive use.

Based on the success story of EP compounds related to Art in malaria treatment (31) and the observation that an essential oil from *Chenopodium ambrosioides* containing the EP Asc is effective against *Leishmania amazonensis* (37), several studies on the potential benefit of natural and synthetic EP against *Leishmania* were performed in the past. These studies revealed that *Leishmania* are exceptionally sensitive to peroxides including EP since they have a high labile iron pool and depending on the nutrient supply by the host macrophages contain also significant amounts of heme (7, 38). These iron compounds are preferential triggers of peroxide activation leading to carbon-centered radicals and ROS. Another aspect, which influences the efficiency of EP in intracellular *Leishmania*, is the effect that in contrast to hydroperoxides cyclic EP has no distinct detoxification pathways in the macrophage of the host cell. However, several studies have shown that the molecular structure of EP beyond the EP group can significantly influence anti-leishmanial efficiency and selectivity. This is quite clear since not only the EP group, but also often the residual part of the molecule will determine the pharmacokinetic distribution and intracellular binding of the EP to specific protein targets.

So far several groups of EP, including Asc and artemisinins, AcEP were studied in the model systems of LtP and J774 macrophages (7, 8, 38).

The literature reports about the antiparasitic activity of a variety of natural EP from various sources, such as marine organisms, fungi and bacteria (39, 40). The major limitation for mechanistic exploration is often the availability of sufficient amounts of compounds. For example for ErgoEP, which was isolated from plants and mushrooms, an activity against *Leishmania* species was reported (32, 41). However, the amounts from natural sources are low and even if commercially available small amounts are very expensive.

Therefore, this work focused on the synthetic preparation of EP from Ergo and DHChol and subsequent evaluation of basic anti-leishmanial activity as well as some mechanistic aspects.

In the first step, it was important to understand the molecular changes by photo-oxidation of both sterols. We have chosen ^{1}H NMR spectroscopy as method to monitor molecular changes. To understand the expected changes in ^{1}H NMR spectra we performed several simulations. The region of the molecules, which is of interest for modification corresponds to alkenes - hydrogen atoms, attached to carbon atoms, which are part of a double bond system. In addition, the chemical shifts of the respective hydrogen atoms are modulated by the presence of heteroatoms or other carbon-carbon double bonds in the vicinity of the respective hydrogen atoms. Therefore, for Ergo we can observe in the ^{1}H NMR spectrum absorptions for two hydrogen atoms at the double bonds in the ring at 6,7-position δ ca 5.9 ppm and in addition from two hydrogen atoms of the aliphatic side chain at δ ca 5.4 ppm (Figure 4). The simulated spectrum of DHChol displays a similar absorption at δ ca 5.9 ppm, but no absorption around δ 5.4 ppm since this molecule has no double bond in the aliphatic side chain (Figure 5). Comparing these simulated shifts with experimental ^{1}H NMR spectra of these molecules, it became visible that qualitatively the spectral patterns were similar, however, the absorptions were appearing at slightly higher values (Table 5). For corresponding EP as well as EP with additional double bonds the absorptions of the two hydrogen atoms at the ring double bond show even higher shift values (Figures 6, 7, 8, 9). Experimental spectra of our synthetic products confirmed this relative effect (Figures 19, 20). This shows that NMR is a suitable tool for product monitoring, however, with certain limitations. While for ^{1}H NMR only about 0.5 mg of substance are required, complete reaction mixtures are sometimes difficult to analyze. Therefore, more economic and rapid reaction monitoring is often done by TLC.

Photo-oxidation reactions are usually based on the principle that a PS, which is irradiated by light (of suitable wavelength), is generating singlet oxygen which then binds to the conjugated double bonds of the respective sterols (Figure 10). Efficiency of this reaction and the product pattern obtained depends on various experimental factors, including type and concentration of the PS, type and intensity of the light irradiation, concentration of oxygen in the solution, temperature, and type of the solvent. All these factors determine the yield and the purity of the respective EP and occurrence of possible side products (Figure 11). Therefore, we selected for the synthesis of every sterol different combinations of PS (MB, EY) and solvent (CH_2Cl_2, EtOH) (Table 3) following suggestions published by Bu et al. (23).

Monitoring of the respective reaction was done by taking aliquots at different time points and subsequent TLC analyzes (Figures 12, 13). Used TLC plates contained a fluorescent indicator with an absorption maximum at 254 nm. Therefore, substances, which interact with this indicator, are visible as differently colored spots. Sterols itself, which are the starting products of the reaction appear as dark violet spots. In contrast, resulting EP possess no conjugated double bonds anymore, therefore, do not strongly interact with the UV illumination and fluorescence emission of the plates, and are nonvisible. In order to make EP visible on TLC plates, we stained these plates with a Fe^{2+}/SCN mixture. The rationale behind this staining is that Fe^{2+} reacts with the peroxides yielding Fe^{3+}, which is forming a dark red complex with SCN. Stainings are shown in figures 15 and 16.

Therefore, in the monitoring procedure, the photochemical reaction was continued until the sterol spots completely disappeared (Figures 12, 13). This was considered as an endpoint of the reaction. After we completed three reaction batches, they were pooled and column chromatography was performed obtaining 21 different fractions. These fractions were again analyzed by TLC chromatography either with UV illumination and Fe^{2+}/SCN staining (figures 14, 15, 16). With this method, we identified those fractions with the highest amounts of EP, which were then analyzed by ^1H NMR spectroscopy (Figures 17, 18, 19, 20).

After integration of the signals of the individual compounds at shifts shown in table 5 the purity of the different fractions was calculated and is shown in tables 6 and 7.

According to these data, we selected the fraction “220301_Ergo_MB_F14“ for ErgoEP and fraction “220331_DHCholEP_MB_F13” for DHCholEP for further studies.

The influence of sterol EP and sterols, as well as reference compounds, on the viability of LtP was studied in resazurin viability assays. Technically speaking, assays in 96-well plates

with vertical (6 concentrations) and horizontal concentration gradients (12 concentrations) were performed (Figures 21, 22). In both types of assays, EP from both sterols show IC_{50} values below 10 µM (Table 8, 9). This is similar to findings in the literature, which report an IC_{50} of ErgoEP against *Trypanosoma cruzi* of 15.5 µM (43). The positive control with Pen shows an IC_{50} value of a few µM, which is in agreement with findings in our previous work (Table 9) (7). The negative control containing Chol shows that this sterol has almost no negative influence on the viability of LtP with an IC_{50} value higher than 200 µM.

Surprisingly, IC_{50} values of Ergo and DHChol in LtP were rather low. Unfortunately, there is no study known which directly compares Ergo to ErgoEP with respect of effects on viability in *Leishmania*.

In general, in both assay types, IC_{50} values of the EP were slightly lower than the values of the corresponding sterols, suggesting that the EP group increases the antileishmanial efficiency.

In addition, we verified whether NAC interferes in the anti-leishmanial effect of sterol EP (Figure 23) (Table 10). Certain anthracene endoperoxides show 2 to 10-fold difference in IC_{50} values when the NAC was introduced in the LtP viability assay (45). In comparison, our experiments show much lower effect of NAC. NAC is a thiol which could act as a reductant of a heme iron, as heme was also present in the assay. This could theoretically lead to the increase in the peroxidal effect, and interfere with the effect of NAC. Unfortunately, the data show a very high standard deviation, but there was a general tendency that for all compounds IC_{50} values were shifted to higher values in the presence of NAC. This indicates that presumably oxidative processes/radical formation are involved in the pharmacological mechanism of these compounds. While this was expected for the EP, this is surprising for Ergo and DHChol itself.

Finally, the reactivity of sterol EP and sterols with Fe^{2+} was studied in the XO assay (Figure 24). While the control compound Chol showed a very low reaction rate, the positive control Asc exhibited reaction rates above 109 nmol/min. Surprisingly not only sterol EP but also sterols (Ergo, DHChol) demonstrated high reaction rates in a biphasic reaction. These compounds initially reacted very fast and then this was followed by a slow-reaction phase.

Based on a literature reference (44), which shows the ability of sterols with conjugated double bonds to undergo iron-catalyzed oxidation, the reaction scheme in Figure 25 was proposed.

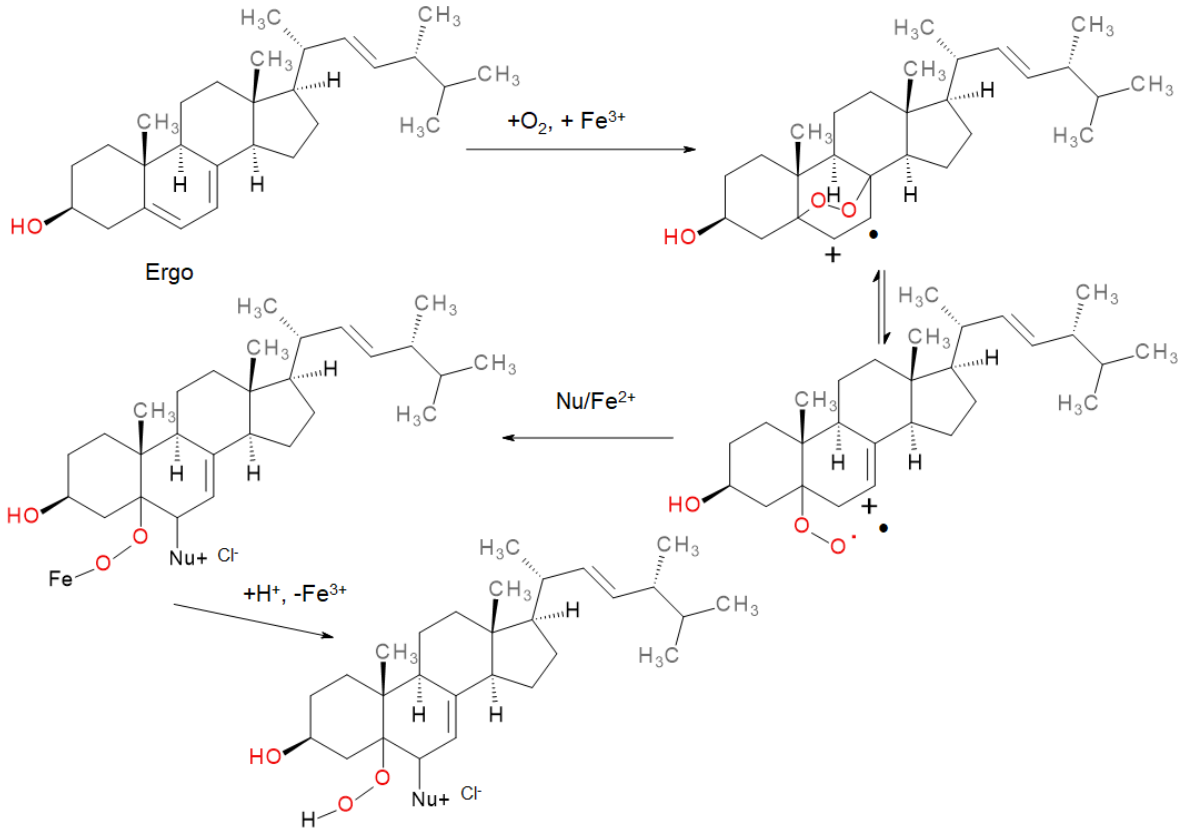

Figure 25. Iron-catalyzed radical formation from Ergo. The upper graph shows the oxidation process of Ergo supported by Fe^{3+} and oxygen, that leads to the formation of a radical cation. This radical cation is unstable, which can lead to the cleavage of endoperoxidic bridge and formation of an additional double bond at 7,8-position. The radical cation in this transitional state acts as an alkylating agent that can be stabilized via the reaction with cellular nucleophiles (Nu) and Fe^{2+}. Fe^{2+} stabilizes the peroxide group, however, it can be substituted with a proton (lower graph). Drawn according to literature reference (44).

This reaction sequence could explain why Ergo and DHChol show a high reaction rate in the XO assay and rather low IC_{50} values (if compared to Chol) for the anti-leishmanial activity. Whether this is a general phenomenon or consequence of the specific set up in our viability assays (containing hemin and thiols in the assay medium), could not be clarified so far. The toxicity of Ergo in *Leishmania* appears to be surprising on the first view since *Leishmania* membranes contain also significant amounts of Ergo (16). On the other hand, the amount of Ergo, which was added in our assays, was not membrane-bound in contrast to Ergo biosynthesized in *Leishmania*. This difference in compartmentalization could play an

important role in the effects we observed. Since all previous studies on the anti-leishmanial effect of ErgoEP did not compare with Ergo, it remains difficult to decide whether our finding is generally valid. Therefore, future research on the anti-leishmanial mechanism of these sterols and corresponding EP is required.

In conclusion, we have shown that sufficiently pure fractions of sterol EP can be synthetized by means of photochemical reactions. The resulting sterol EP show significant anti-leishmanial activity, however, the actual molecular targets in *Leishmania* and host macrophages need to be explored in future research.

5. Summary

Leishmaniasis is a vector-borne disease caused by an intracellular parasite *Leishmania spp.*, transmitted through a vector (sandfly). Therefore, the occurrence of the disease is connected to the natural habitat of a sandfly. Considering it being endemic in 98 countries, it is a widespread disease and a global health problem. Endoperoxides (EP) possess the ability to avoid the cellular detoxification pathways in host cells, allowing them to also exhibit their cytotoxic properties on intracellular *Leishmania.* Their antileishmanial potency is supported by the fact that they tend to be activated via the reaction with Fe^{2+} turning them into radicals. This is favoured since *Leishmania spp.* possess a high labile iron pool and get a sufficient iron supply from their surrounding. In this bachelor thesis, the synthesis and the antileishmanial effects of sterol endoperoxides ergosterol EP, and 7-dehydrocholesterol EP, were examined.

The goal was to establish a method that could lead to high yields and purity of the product. Afterwards, the products were studied in viability assays, where the IC_{50} values for *Leishmania tarentolae* promastigotes were determined.

Our synthethic approach based on different irradiation times, solvent combinations and photosensitizers yielded an EP purity up to 96.2 %. This allowed us to carry out the viability assays with high-quality products and provided reliable results. IC_{50} values for EP lower than 10 µM were measured during our experiments, which showed that the antileishmanial properties of sterol EP are higher compared to respective sterols. The viability assays in the presence of the radical scavenger N-acetyl cysteine showed that it is highly likely that the antileishmanial effects of sterol EP rely on their transformation into radicals by single electron reduction. A reaction of our products with xylenol orange and Fe^{2+}, which was spectrophotometrically evaluated, was conducted to determine if this transition into radicals is influenced by the reaction with Fe^{2+}. The reaction rates of the EP obtained during the experiment indicate that there is a high possibility of Fe^{2+} activation not only for sterol EP, but for sterols as well.
During this work we have managed to obtain important data regarding the production process of sterol EP, as well as the background of their antileishmanial activity.

6. Abbreviations

AcEP	...	anthracene endoperoxides
Art	...	artemisinin
Asc	...	ascaridole
BHI	...	brain heart infusion
BHT	...	butylated hydroxytoluene
Cin	...	1,4-cineole
CL	...	cutaneous leishmaniasis
DHChol	...	7-dehydrocholesterol
DHCholEP	...	7-dehydrocholesterol peroxide
DHErgoEP	...	dehydroergosterol peroxide
DMSO	...	dimethyl sulfoxide
EP	...	endoperoxides
Ergo	...	ergosterol
ErgoEP	...	ergosterol peroxide
EtOAc	...	ethyl acetate
EtOH	...	ethanol
EY	...	eosin Y
Glu	...	glucose monohydrate
IC_{50}	...	half maximal inhibitory concentration
$LOO^{\cdot}$	...	lipid peroxyl radicals
LtP	...	*Leishmania tarentolae* promastigotes
MB	...	methylene blue
MCL	...	mucocutaneous leishmaniasis
MeOH	...	methanol
NAC	...	N-acetyl cysteine
NMR	...	nuclear magnetic resonance
OD	...	optical density
PBS	...	phosphate-buffered saline
PE	...	petroleum ether
Pen	...	pentamidine
PS	...	photosensitizer

ROS	...	reactive oxygen species
SSG	...	sodium stibogluconate
TDHCholEP	...	tetra-dehydrocholesterol peroxide
TLC	...	thin-layer chromatography
UV-Vis	...	ultraviolet-visible spectroscopy
VL	...	visceral leishmaniasis
VLC	...	vacuum liquid chromatography
WHO	...	World Health Organization
XO	...	xylenol orange
YE	...	yeast extract

7. References

1. Kaye P, Scott P. Leishmaniasis: complexity at the host–pathogen interface. Nature Reviews Microbiology. 2011 Aug 11;9(8):604–15.
2. Teixeira DE, Benchimol M, Rodrigues JCF, Crepaldi PH, Pimenta PFP, de Souza W. The cell biology of *Leishmania*: how to teach using animations. PLoS Pathogens. 2013 Oct 10;9(10):e1003594.
3. Zulfiqar B, Shelper TB, Avery VM. Leishmaniasis drug discovery: recent progress and challenges in assay development. Drug Discovery Today. 2017 Oct;22(10):1516–31.
4. Croft SL, Coombs GH. Leishmaniasis– current chemotherapy and recent advances in the search for novel drugs. Trends in Parasitology. 2003 Nov;19(11):502–8.
5. Frézard F, Demicheli C, Ribeiro R. Pentavalent antimonials: new perspectives for old drugs. Molecules. 2009 Jun 30;14(7):2317–36.
6. Alvar J, Arana B. I. Appraisal of leishmaniasis chemotherapy, current status and pipeline strategies. Chapter 1. Leishmaniasis, Impact and Therapeutic Needs. Drug Discovery for Leishmaniasis. 2017. p. 1–23.
7. Geroldinger G, Tonner M, Hettegger H, Bacher M, Monzote L, Walter M, et al. Mechanism of ascaridole activation in *Leishmania*. Biochemical Pharmacology. 2017 May;132:48–62.
8. Geroldinger G, Tonner M, Fudickar W, de Sarkar S, Dighal A, Monzote L, et al. Activation of anthracene endoperoxides in *Leishmania* and impairment of mitochondrial functions. Molecules. 2018 Jul 10;23(7):1680.
9. Mach J, Sutak R. Iron in parasitic protists – from uptake to storage and where we can interfere. Metallomics. 2020 Sep 1;12(9):1335–47.
10. Wei JH, Yin X, Welander P v. Sterol synthesis in diverse bacteria. Frontiers in Microbiology. 2016 Jun 24;7:990.
11. Sterol [Internet]. Wikipedia.org. 2021 [updated 2021 Dec 13; cited 2022 Jul 25]. Available from: https://en.wikipedia.org/wiki/Sterol
12. Ostlund RE, Racette SB, Stenson WF. Inhibition of cholesterol absorption by phytosterol-replete wheat germ compared with phytosterol-depleted wheat germ. The American Journal of Clinical Nutrition. 2003 Jun 1;77(6):1385–9.
13. Murphy RC, Johnson KM. Cholesterol, reactive oxygen species, and the formation of biologically active mediators. Journal of Biological Chemistry. 2008 Jun;283(23):15521–5.
14. Solanko KA, Modzel M, Solanko LM, Wüstner D. Fluorescent sterols and cholesteryl esters as probes for intracellular cholesterol transport. Lipid Insights. 2015 Jan 9;8s1:95–114.
15. Magaraci F, Jimenez, Rodrigues C, Rodrigues JCF, Braga MV, Yardley V, et al. Azasterols as inhibitors of sterol 24-methyltransferase in *Leishmania* species and *Trypanosoma cruzi*. Journal of Medicinal Chemistry. 2003 Oct 1;46(22):4714–27.

16. Yao C, Wilson ME. Dynamics of sterol synthesis during development of *Leishmania spp.* parasites to their virulent form. Parasites & Vectors. 2016 Dec 12;9(1):200.

17. Parsi Z, Górecki T. Determination of ergosterol as an indicator of fungal biomass in various samples using non-discriminating flash pyrolysis. Journal of Chromatography A. 2006 Oct;1130(1):145–50.

18. Deluca HF. The genetics and biology of vitamin D. 1997. p. 617–41.

19. Dionisio KL, Phillips K, Price PS, Grulke CM, Williams A, Biryol D, et al. The Chemical and products database, a resource for exposure-relevant data on chemicals in consumer products. Scientific Data. 2018 Dec 10;5(1):180125.

20. Zerbinati C, Iuliano L. Cholesterol and related sterols autoxidation. Free Radical Biology and Medicine. 2017 Oct;111:151–5.

21. Lagunes I, Trigos Á. Photo-oxidation of ergosterol: indirect detection of antioxidants photosensitizers or quenchers of singlet oxygen. Journal of Photochemistry and Photobiology B: Biology. 2015 Apr;145:30–4.

22. Trigos Á, Mendoza G, Espinoza C, Salinas A, Fernández JJ, Norte M. The role of macrosporin in necrotic spots. Phytochemistry Letters. 2011 Jun;4(2):122–5.

23. Bu M, Cao T, Li H, Guo M, Yang BB, Zhou Y, et al. Synthesis and biological evaluation of novel steroidal 5α,8α-endoperoxide derivatives with aliphatic side-chain as potential anticancer agents. Steroids. 2017 Aug;124:46–53.

24. Ferrié L. Advances in the synthesis of 1,2-dioxolanes and 1,2-dioxanes. 2021. p. 57–146.

25. Cateni F, Doljak B, Zacchigna M, Anderluh M, Piltaver A, Scialino G, et al. New biologically active epidioxysterols from *Stereum hirsutum*. Bioorganic & Medicinal Chemistry Letters. 2007 Nov;17(22):6330–4.

26. Ling T, Lang WH, Martinez-Montemayor MM, Rivas F. Development of ergosterol peroxide probes for cellular localisation studies. Organic & Biomolecular Chemistry. 2019;17(21):5223–9.

27. Tian N na, Li C, Tian N, Zhou Q xiong, Hou Y jun, Zhang B wen, et al. Syntheses of 7-dehydrocholesterol peroxides and their improved anticancer activity and selectivity over ergosterol peroxide. New Journal of Chemistry. 2017;41(24):14843–6.

28. Li X, Wu Q, Bu M, Hu L, Du WW, Jiao C, et al. Ergosterol peroxide activates Foxo3-mediated cell death signaling by inhibiting AKT and c-Myc in human hepatocellular carcinoma cells. Oncotarget. 2016 Jun 7;7(23):33948–59.

29. Martin Piontek. Antileishmanial efficiency and mechanism of anthracene endoperoxides [Bachelor thesis]. [Vienna]: University of Veterinary Medicine; 2019.

30. Leishmaniasis [Internet]. PAHO/WHO | Pan American Health Organization. [cited 2022 Jul 25]. Available from: https://www.paho.org/en/topics/leishmaniasis

31. Maude RJ, Woodrow CJ, White LJ. Artemisinin antimalarials: preserving the „magic bullet“. Drug Development Research. 2010 Feb;71(1):12–19.

32. Cantrell CL, Rajab MS, Franzblau SG, Fronczek FR, Fischer NH. Antimycobacterial ergosterol-5,8-endoperoxide from *Ajuga remota*. Planta Medica. 1999 Dec;65(8):732–4.

33. Sara Todhe. Antileishmanial action of endoperoxides [Bachelor thesis]. [Vienna]: University of Veterinary Medicine; 2021.

34. Banfi D, Patiny L. www.nmrdb.org: resurrecting and processing NMR spectra on-line. CHIMIA. 2008 Apr 30;62(4):280.

35. Castillo AM, Patiny L, Wist J. Fast and accurate algorithm for the simulation of NMR spectra of large spin systems. Journal of Magnetic Resonance. 2011 Apr;209(2):123–30.

36. Aires-de-Sousa J, Hemmer MC, Gasteiger J. Prediction of ^{1}H NMR Chemical Shifts Using Neural Networks. Analytical Chemistry. 2002 Jan 1;74(1):80–90.

37. Monzote L, Montalvo AM, Almanonni S, Scull R, Miranda M, Abreu J. Activity of the essential oil from *Chenopodium ambrosioides* grown in Cuba against *Leishmania amazonensis*. Chemotherapy. 2006;52(3):130–6.

38. Geroldinger G, Tonner M, Quirgst J, Walter M, de Sarkar S, Machín L, et al. Activation of artemisinin and heme degradation in *Leishmania tarentolae promastigotes*: a possible link. Biochemical Pharmacology. 2020 Mar;173:113737.

39. Fontana A, Cimino G, Gavagnin M, González MC, Estornell E. Novel inhibitors of mitochondrial respiratory chain: endoperoxides from the marine tunicate *Stolonica socialis*. Journal of Medicinal Chemistry. 2001 Jul 1;44(14):2362–5.

40. Dembitsky VM. Bioactive peroxides as potential therapeutic agents. European Journal of Medicinal Chemistry. 2008 Feb;43(2):223–51.

41. Merdivan S, Lindequist U. Ergosterol peroxide: a mushroom-derived compound with promising biological activities - a review. International Journal of Medicinal Mushrooms. 2017;19(2):93–105.

42. Adam HK, Campbell IM, McCorcindale NJ. Ergosterol peroxide: a fungal artefact. Nature. 1967 Oct 1;216(5113):397–397.

43. Ramos-Ligonio A, López-Monteon A, Trigos Á. Trypanocidal activity of ergosterol peroxide from *Pleurotus ostreatus*. Phytotherapy Research. 2012 Jun;26(6):938–43.

44. Wilk M, Schmitt K. Activation of steroid systems to alkylating agents. Zeitschrift für Naturforschung B. 1981 Feb 1;36(2):248–51.

45. Machin L, Piontek M, Todhe S, Staniek K, Monzote L, Fudickar W, et al. Antileishmanial anthracene endoperoxides: efficacy in vitro, mechanisms and structure-activity relationships. Molecules 2022;27(20).

8. List of figures

Figure 1. Life cycle of *Leishmania*. 5
Figure 2. Structures and abbreviations of sterol EP, their analogs, as well as the control substances used in the experiments. 13
Figure 3. Experimental setup for VLC. 17
Figure 4. Simulated ^{1}H NMR spectrum of Ergo. 20
Figure 5. Simulated ^{1}H NMR spectrum of DHChol. 21
Figure 7. Simulated ^{1}H NMR spectrum of DHCholEP. 23
Figure 8. Simulated ^{1}H NMR spectrum of DHErgoEP. 24
Figure 9. Simulated ^{1}H NMR spectrum of TDHCholEP. 25
Figure 10. Reaction scheme of photo-oxidation of Ergo and DHChol to their corresponding EP. 26
Figure 11. Possible side products of photo-oxidation of sterols. 26
Figure 12. Typical TLC plate of the reaction of Ergo with O_2 in the presence of MB visualized by UV illumination. 28
Figure 13. Typical TLC plate of the reaction of DHChol with O_2 in the presence of MB visualized by UV illumination. 29
Figure 14. Typical TLC plate of fractions obtained by VLC purification of reaction products of DHChol with O_2 in the presence of MB visualized by UV illumination. 30
Figure 15. Typical TLC plate of fractions obtained by VLC purification of reaction products of DHChol with O_2 in the presence of MB visualized by Fe^{2+}/SCN staining. 31
Figure 16. Typical TLC plate of fractions 8-14 obtained by VLC purification of reaction products of Ergo with O_2 in the presence of MB visualized by Fe^{2+}/SCN staining. 32
Figure 17. Experimental ^{1}H NMR spectrum of Ergo. 33
Figure 18. Experimental ^{1}H NMR spectrum of DHChol. 33
Figure 19. Experimental ^{1}H NMR spectrum of a purified product of Ergo photo-oxidation. 34
Figure 20. Experimental ^{1}H NMR spectrum of a purified product of DHChol photo-oxydation. 35
Figure 21. Typical viability-concentration curve for LtP as a function of different concentrations of ErgoEP (0.097 µM to 200 µM) in 96-well plates with vertical concentration gradients. 37

Figure 22. Typical viability-concentration curve for LtP as a function of different concentrations of DHCholEP (0.082 µM to 200 µM) in 96-well plates with horizontal concentration gradients. 38
Figure 23. Typical viability-concentration curves for LtP as a function of different concentrations of ErgoEP without (left) and with (right) the addition of 2 mM NAC to the media. 39
Figure 24. Visual spectra of the formation (lowest trace at t = 0 s) of the Fe^{3+}/XO complex from the reaction of Asc (100 µM) with Fe^{2+} (250 µM) dissolved in MeOH/H_2O (9:1) in the presence of XO and air. 41
Figure 25. Iron-catalyzed radical formation from Ergo. 46

9. List of tables

Table 1. List of the chemicals used for preparation, maintenance and synthetic processes . 12
Table 2. VLC Fractions with the corresponding solvent mixture for each fraction. 18
Table 3. Variants of synthesis performed for photo-oxidation of sterols. 27
Table 4. Typical example of the samples taken for the TLC analysis during the DHCholEP synthetic process. 29
Table 5. ^{1}H NMR shifts of H at ring double bonds in sterols and corresponding EP. 35
Table 6. Purity and amount of synthesized fractions from Ergo. 35
Table 7. Purity and amount of synthesized fractions from DHChol. 36
Table 8. Influence of sterols (Ergo, DHChol) and corresponding peroxides (ErgoEP, DHCholEP) on the viability of LtP in 96-well plates with vertical concentration gradients (6 concentrations). 37
Table 9. Influence of sterols (Ergo, DHChol), corresponding peroxides (ErgoEP, DHCholEP) and reference compound (Pen) on the viability of LtP in 96-well plates with horizontal concentration gradients (12 concentrations). 38
Table 10. Influence of NAC (2 mM) on IC_{50} values of sterols and corresponding peroxides on the viability of LtP in 96-well plates with vertical concentration gradients (6 concentrations). 40
Table 11. Formation rates of the Fe^{3+}/XO complex. The OD increase at 560 nm over time was determined using a spectrophotometer. 41